

FLUID SOLVER INDEPENDENT HYBRID METHODS FOR MULTISCALE KINETIC EQUATIONS*

GIACOMO DIMARCO[†] AND LORENZO PARESCHI[‡]

Abstract. In some recent works [11, 12] we developed a general framework for the construction of hybrid algorithms which are able to face efficiently the multiscale nature of some hyperbolic and kinetic problems. Here, at variance with respect to the previous methods, we construct a method form-fitting to any type of finite volume or finite difference scheme for the reduced equilibrium system. Thanks to the coupling of Monte Carlo techniques for the solution of the kinetic equations with macroscopic methods for the limiting fluid equations, we show how it is possible to solve multiscale fluid dynamic phenomena faster with respect to traditional deterministic/stochastic methods for the full kinetic equations. In addition, due to the hybrid nature of the schemes, the numerical solution is affected by less fluctuations when compared to standard Monte Carlo schemes. Applications to the Boltzmann-BGK equation are presented to show the performance of the new methods in comparison with classical approaches used in the simulation of kinetic equations.

Keywords: multiscale problems, hybrid methods, Boltzmann-BGK equation, Euler equation, Monte Carlo methods, fluid-dynamic limit.

1. Introduction. The classical fluid dynamic models like the Navier-Stokes or the Euler equations are not always satisfactory when dealing with large temperature or very low densities, and a more detailed analysis becomes often necessary to obtain correct values of the macroscopic quantities. In such cases a kinetic approach based on the Boltzmann equation [5] is used. The introduction of such a model is closely linked with the introduction of strong difficulties from the numerical and computational point of view. In fact, the system of equations to solve becomes very large, especially in multidimensional situations, and even with computers of the last generation the computational cost of a direct discretization is often prohibitive. Moreover the Boltzmann collision term that characterizes the kinetic equation, is very hard to treat in practice due to its nonlinear nature and physical properties. To these aims, probabilistic techniques such as Direct Simulation Monte Carlo (DSMC) are extensively used in real simulations for their great flexibility, capability of treating different collision terms and low computational cost compared to deterministic schemes for kinetic equations [1, 3, 20, 22]. On the other hand solutions are affected by large fluctuations and, in non stationary situations, the difficulty to compute averaged quantities leads to low accurate solutions or very expensive simulations. However, even in extremely rarefied regimes the fluid dynamic equations still furnish correct solution in regions of the domain where the gas is not subjected to sharp gradient. The direct consequence is that domain decomposition methods [2, 19, 10] which consider the problem at different scales, fluid or kinetic, in different part of the computational domain, is a practical way to take advantage of the physics without loosing accuracy. We quote also the possibility to improve domain decomposition schemes through a moving boundary [9, 32], in order to follow discontinuities and sharp gradients inside the domain, these methods are particularly important in the simulation of non stationary problems. Clearly, the exact identification of the non equilibrium zones remains an hard task to deal with and an open research argument.

In some recent works we proposed an alternative approach to domain decomposition methods based on the use of different numerical methods on the whole computational domain [11, 12]. We mention here that similar hybrid approaches have been considered in [7, 14, 15, 22, 31]. Even if we develop our methods in the case of rarefied gas dynamics (RGD) the formulation we proposed per-

*This work was partially supported by the INDAM project “Kinetic Innovative Models for the Study of the Behavior of Fluids in Micro/nano Electromechanical Systems”

[†] University of Ferrara, Department of Mathematics and CMCS, Ferrara, Italy (Giacomo.Dimarco@unife.it).

[‡] University of Ferrara, Department of Mathematics and CMCS, Ferrara, Italy (Lorenzo.Pareschi@unife.it).

mits easily generalizations to others fields in which kinetic and hyperbolic multiscale phenomena are present. In order to use the hybrid approach here described, it is essential to identify a local equilibrium function, like the Maxwellian distribution for RGD, either analytically or numerically. This local equilibrium originates a model reduction from the microscale to the macroscale formulation and allows to ignore the details of microscopic interactions in terms of simplified equations which describe the equilibrium system.

The schemes here presented represent an important improvement with respect to the schemes developed in [11, 12] where the limiting equilibrium method was limited by construction to a kinetic scheme. In the present work we generalize the approach to make the method independent of the fluid solver used. We point out that this generalization is not trivial since in an arbitrary fluid solver we miss the kinetic information on the distribution function which is present in a standard kinetic scheme. The main advantage is that the method in the fluid limit degenerates into a standard fluid solver without any additional cost of a kinetic simulation. To our knowledge this is the first method which satisfy this property for RGD.

Although we will focus, in the construction of the schemes, on the simplified BGK collision model, in principle the schemes can be extended to the full Boltzmann collision operator through the use of time relaxed Monte Carlo methods [21, 22, 23, 24]. The basic idea consists in solving the kinetic model and the macroscopic model in the entire domain, the first through Monte Carlo techniques which are robust in the fluid limit and the latter through a deterministic scheme and to consider as a solution a suitable hybrid merging of the two. A remarkable feature of the new method is the use of the hybrid moments to correct the stochastic moments in the pure Monte Carlo scheme. This is an important source of fluctuations reduction in the method.

In addition we will show that it is not necessary to keep the number of sample particles fixed in the Monte Carlo scheme, instead it is sufficient to describe at the particles level only the fraction of the solution which is far from the thermodynamic equilibrium. The immediate consequence of the above observation is a potential reduction of the number of samples used in the Monte Carlo solution, and thereby, of computational time and fluctuations. These improvements are directly linked with the decrease of the local Knudsen number which is a measure of the rarefaction of the gas. The implementation of such methodology produces numerical schemes which, in general, are much faster than deterministic kinetic schemes and, for flow regimes close to the fluid limit, also to DSMC schemes. Moreover, thanks to the general formulation of the algorithm, a domain decomposition technique can be directly derived forcing the Knudsen number to zero (see [13]) in some regions of the domain.

Finally, let us observe that the method here developed is based on the classical operator splitting for the kinetic equation. This is essential if one want to match the fluid scheme with standard DSMC solvers for RGD, since the latter are based on such splitting. Even if there are well-known limitations of such splitting when dealing with Navier-Stokes asymptotics, namely the time step has to be related to the Knudsen number in order to describe correctly the Navier-Stokes level [33], here we don't aim at an under-resolved method at all the scales but simply at developing a method which is asymptotic preserving (AP) in the stiff limit [16]. On the other hand the advantages provided by our final method in terms of fluctuations and computational cost reduction are essentially independent of the small scales resolution but depend only on the Knudsen number. Note that in principle one can improve the method coupling the DSMC solver with a Navier-Stokes fluid description instead of a Euler one. This coupling however is not straightforward and we don't explore this direction here.

The rest of the article is organized as follows. In Section 2 we introduce the BGK equations and his properties. In Section 3 we recall the general structure of the hybrid methods derived in [11, 12]. Next in Section 4 the fluid solver independent hybrid scheme is described together with an acceleration technique and two possible ways in which the equilibrium fraction can be increased.

Section 5 is devoted to numerical results to compare performances respect traditional Monte Carlo and kinetic schemes. Some final considerations and future developments are discussed in the last Section.

2. The Boltzmann-BGK Model. We consider the following Boltzmann-BGK kinetic model

$$\partial_t f(x, v, t) + v \cdot \nabla_x f(x, v, t) = \frac{1}{\tau(x, t)} (M_f(x, v, t) - f(x, v, t)), \quad (2.1)$$

with the initial condition

$$f(x, v, t = 0) = f_0(x, v). \quad (2.2)$$

In (2.1) the function $f(x, v, t)$ is non negative and describes the time evolution of the distribution of particles with velocity $v \in \mathbb{R}^d$ and position $x \in \Omega \subset \mathbb{R}^D$, with d and D representing the dimension in velocity and physical space respectively. In this simplified model the Boltzmann collision term is substituted by a relaxation towards equilibrium. In the sequel we will work with nondimensional quantities, in that case τ , the relaxation frequency, can be written as

$$\tau(x, t)^{-1} = \frac{C}{\varepsilon(x, t)}, \quad (2.3)$$

where $\varepsilon(x, t)$ is the Knudsen number. Here we assume $C = 1$ [6, 27]. Others choices of the relaxation time do not change the hybrid algorithm we will describe in next section. Observe anyway that the ratio of deterministic and stochastic component will be a function of the relaxation time, being linked to the ratio of the distribution function with respect to the Maxwellian equilibrium function as explained in details in the next Section. In the following, for simplicity, we will skip the space and time dependency of the Knudsen number thus $\varepsilon(x, t) = \varepsilon$.

The local Maxwellian function, representing the local equilibrium, is defined by

$$M_f(\varrho, u, T)(x, v, t) = \frac{\varrho}{(2\pi T)^{d/2}} \exp\left(\frac{-|u - v|^2}{2T}\right), \quad (2.4)$$

where ϱ , u , T are the density, mean velocity and temperature of the gas in the x -position and at time t

$$\varrho = \int_{\mathbb{R}^d} f dv, \quad u = \frac{1}{\varrho} \int_{\mathbb{R}^d} v f dv, \quad T = \frac{1}{d\varrho} \int_{\mathbb{R}^d} |v - u|^2 f dv, \quad (2.5)$$

while the energy E is defined as

$$E = \frac{1}{2} \int_{\mathbb{R}^d} |v|^2 f dv. \quad (2.6)$$

Consider now the BGK equation (2.1) and multiply it for 1 , v , $\frac{1}{2}|v|^2$, the so-called collision invariant. By integrating in v the above quantities, the equations for the first three moments of the distribution function f are obtained. They describe respectively the conservations laws for mass, momentum and energy. Unfortunately, the system obtained through the above average in velocity space is not closed since it involves higher order moments of the distribution function.

Note that, formally from (2.1) as $\varepsilon \rightarrow 0$, the function f approaches the local Maxwellian. In this case it is possible to compute analytically the higher moments of f from ϱ , u and T . Carrying on this computation we obtain the set of compressible Euler equations (see [4] for details)

$$\begin{aligned}
\frac{\partial \varrho}{\partial t} + \nabla_x \cdot (\varrho u) &= 0 \\
\frac{\partial \varrho u}{\partial t} + \nabla_x \cdot (\varrho u \otimes u + p) &= 0, \\
\frac{\partial E}{\partial t} + \nabla_x \cdot (Eu + pu) &= 0 \\
p = \varrho T, \quad E = \frac{d}{2} \varrho T + \frac{1}{2} \varrho |u|^2 &
\end{aligned} \tag{2.7}$$

where p is the thermodynamical pressure while \otimes represents a tensor product. Higher order fluid model, like Navier-Stokes, can be derived similarly [4].

3. Hybrid Methods. The schemes derived in this paper are based on the same hybrid representation defined in [12]. Here we recall only the key points of the previous method, for details we remind to [12].

For a fixed space point x we can interpret the distribution function as a probability density in the velocity space (the x -dependence is omitted)

$$f(v, t) \geq 0, \quad \varrho = \int_{-\infty}^{+\infty} f(v, t) dv = 1. \tag{3.1}$$

Next we recall the following definition of hybrid representation [12]

DEFINITION 3.1. *Given a probability density $f(v, t)$, and a probability density $M_f(v, t)$, called equilibrium density, we define $w(v, t) \in [0, 1]$ and $\tilde{f}(v, t) \geq 0$ in the following way*

$$w(v, t) = \begin{cases} \frac{f(v, t)}{M_f(v, t)}, & f(v, t) \leq M_f(v, t) \neq 0 \\ 1, & f(v, t) \geq M_f(v, t) \end{cases} \tag{3.2}$$

and

$$\tilde{f}(v, t) = f(v, t) - w(v, t)M_f(v, t). \tag{3.3}$$

Thus $f(v, t)$ can be represented as

$$f(v, t) = \tilde{f}(v, t) + w(v, t)M_f(v, t). \tag{3.4}$$

If we take now $\beta(t) = \min_v \{w(v, t)\}$ and $\tilde{f}(v, t) = f(v, t) - \beta(t)M_f(v, t)$ we have

$$\int_v \tilde{f}(v, t) dv = 1 - \beta(t).$$

Let us define for $\beta(t) \neq 1$ the probability density

$$f^p(v, t) = \frac{\tilde{f}(v, t)}{1 - \beta(t)}.$$

The case $\beta(t) = 1$ is trivial since it implies $f(v, t) = M_f(v, t)$. Thus the probability density $f(v, t)$, can be written as a convex combination of two probability densities in the form [21, 22]

$$f(v, t) = (1 - \beta(t))f^p(v, t) + \beta(t)M_f(v, t). \tag{3.5}$$

Clearly the above representation is a particular case of (3.4).

Now we consider the following general representation, including space dependence

$$f(x, v, t) = \tilde{f}(x, v, t) + w(x, v, t)M_f(x, v, t), \quad (3.6)$$

where $w(x, v, t) \geq 0$ is a function that characterizes the equilibrium fraction and $\tilde{f}(x, v, t)$ the non equilibrium part of the distribution function. This representation in general can be obtained for the initial data of the kinetic equation using directly Definition 1.

The starting point of the method is the classical operator splitting which consists in solving first a homogeneous relaxation step

$$\partial_t f^r(x, v, t) = -\frac{1}{\varepsilon}(f^r(x, v, t) - M^r(x, v, t)) \quad (3.7)$$

and then a free transport equation

$$\partial_t f^c(x, v, t) + v \cdot \nabla_x f^c(x, v, t) = 0. \quad (3.8)$$

In a single time step Δt the computation of the hybrid method derived in [12] can be summarized as follows

- Starting from a function $f^r(x, v, t) = f(x, v, t)$ in the form (3.6) solve the relaxation step (3.7) either analytically or with a suitable numerical time integrator for stiff ODEs, like backward Euler. This originates the decomposition

$$\begin{aligned} f^r(x, v, t + \Delta t) &= \lambda f^r(x, v, t) + (1 - \lambda)M_f(x, v, t) \\ &= \lambda \tilde{f}(x, v, t) + (1 - \lambda + \lambda w(x, v, t))M_f(x, v, t), \end{aligned}$$

with $0 \leq \lambda = \lambda(\Delta t/\varepsilon) \leq 1$ a scheme dependent constant such that $\lambda \rightarrow 0$ as $\Delta t/\varepsilon \rightarrow \infty$. This decomposition can be cast again in the form (3.6) taking $\tilde{f}^r(x, v, t + \Delta t) = \lambda \tilde{f}(x, v, t)$ and $w^r(x, v, t + \Delta t) = 1 - \lambda + \lambda w(x, v, t)$.

1. The new value $w^r(x, v, t + \Delta t)$ follows directly from the choice of λ , so from the time solver used for (3.7).
 2. The new value $\tilde{f}^r(x, v, t + \Delta t)$ is computed by a Monte Carlo method simply discarding a fraction of the samples since $0 \leq \lambda \leq 1$ and so $w^r(x, v, t + \Delta t) \geq w(x, v, t)$.
- Starting from the function $f^c(x, v, t) = \tilde{f}^r(x, v, t + \Delta t)$ in the form (3.6) computed above solve the transport step (3.8).
 1. Transport the particle fraction $\tilde{f}^c(x, v, t)$ by simple particles shifts.
 2. Transport the deterministic fraction $w^c(x, v, t)M_f(x, v, t)$ by a deterministic scheme.
 3. Project the computed hybrid solution $f(x, v, t + \Delta t)$ to the form (3.6) using Definition 1.

Clearly point 3 of the transport step is crucial for the details of the hybrid method. Note that point 2 of the transport step involves the solution of a so-called kinetic scheme for the Euler equations[8, 28].

In the sequel we will describe the Fluid Solver Independent (FSI) schemes which remove the limitations given by the use of a kinetic scheme. One major difference with respect to the hybrid scheme described above is that a common value for the equilibrium fraction in velocity space has to be chosen $\beta(x, t) = \min_v \{w(x, v, t)\}$.

4. Fluid Solver Independent Hybrid Methods. The key feature of FSI methods is to take advantage from the solution of the equilibrium part of the distribution function through a macroscopic scheme instead of a kinetic scheme. Besides its generality, this new feature, could, in principle, lead to a strong reduction of the computational time with respect to any kinetic scheme for the fluid equation.

In order to describe the FSI method we introduce the projection operator \mathcal{P} , and, in a time step Δt , the relaxation operator $\mathcal{R}_{\Delta t}$ and the transport operator $\mathcal{T}_{\Delta t}$. The projection operator computes from the kinetic variable f (or M_f) the macroscopic averages $U(x, t) = (\varrho(x, t), \rho u(x, t), E(x, t))$, thus

$$\mathcal{P}(f(x, v, t)) = U(x, t), \quad \mathcal{P}(M_f(x, v, t)) = U(x, t), \quad (4.1)$$

since the local Maxwellian M_f has the same moments of the distribution function f . The relaxation and transport operators solve the relaxation and transport steps. The first has the form

$$\mathcal{R}_{\Delta t}(f(x, v, t)) = \lambda f(x, v, t) + (1 - \lambda)M_f(x, v, t), \quad (4.2)$$

where $\lambda = \exp(-\Delta t/\varepsilon)$, whereas the second reads

$$\mathcal{T}_{\Delta t}(f(x, v, t)) = f(x - v\Delta t, v, t). \quad (4.3)$$

Similarly we have the approximated relaxation and transport operators \mathcal{R}_a and \mathcal{T}_a . For simplicity, since their particular structure does not play any role in the general derivation of the method, we assume in the sequel that $\mathcal{T}_a = \mathcal{T}$ and $\mathcal{R}_a = \mathcal{R}$. Note that by definition $\mathcal{R}_{\Delta t}(M_f) = M_f$ and so $\mathcal{P}(\mathcal{R}_{\Delta t}(M_f)) = \mathcal{P}(M_f)$.

4.1. A simple FSI method. Let us start from an hybrid solution in the form

$$f(x, v, t) = (1 - \beta(x, t))f^p(x, v, t) + \beta(x, t)M_f(x, v, t), \quad (4.4)$$

where $f^p(x, v, t)$ is represented by samples so that

$$(1 - \beta(x, t))f^p(x, v, t) = m^p \sum_{j=1}^{N(t)} \delta(x - p_j(t))\delta(v - \nu_j(t)), \quad (4.5)$$

where $p_j(t)$ and $\nu_j(t)$ represent the particles position and velocity, and

$$m^p = \frac{1}{N(0)} \int_{\mathbb{R}^d} \int_{\mathbb{R}^D} f(x, v, 0) dx dv$$

is the mass of a single particle, while $M_f(x, v, t)$ is represented analytically. Note that $N(t)$, namely the total number of samples is a function of time since we keep m^p constant during the simulation. This is a crucial feature of the method since if we increase $\beta(x, t)$ in the representation above we must decrease the number of samples $N(t)$. In practice this implies that we will not be able to represent exactly the fraction $\beta(x, t)$ but only its approximation corresponding to integer sums of particles.

Since, as described in the previous section, the first relaxation step has only the consequence of a change of $\beta(x, t)$ in (4.4) we derive the method starting from the transport step.

The transport step produces the solution

$$\mathcal{T}_{\Delta t}(f(x, v, t)) = (1 - \beta(x - v\Delta t, t))f^p(x - v\Delta t, v, t) + \beta(x - v\Delta t, t)M_f(x - v\Delta t, v, t).$$

From a practical viewpoint $(1 - \beta(x - v\Delta t, t))f^p(x - v\Delta t, v, t)$ corresponds to solve a simple particle shift for the Monte Carlo samples. At variance the term $\beta(x - v\Delta t, t)M_f(x - v\Delta t, v, t)$ corresponds to a Maxwellian shift analogous to that usually performed in the so called kinetic or Boltzmann schemes for the Euler equations [8, 28]. The hybrid solution for the moments $U^H(x, t + \Delta t)$ is then recovered as

$$\begin{aligned} U^H(x, t + \Delta t) &= \mathcal{P}(\mathcal{T}_{\Delta t}(f(x, v, t))) \\ &= \mathcal{P}(\mathcal{T}_{\Delta t}((1 - \beta(x, t))f^p(x, v, t))) + \mathcal{P}(\mathcal{T}_{\Delta t}(\beta(x, t)M_f(x, v, t))) \\ &= U^p(x, t + \Delta t) + U^K(x, t + \Delta t). \end{aligned}$$

In particular $U^K(x, t + \Delta t)$ corresponds exactly to the approximation of the Euler solution provided by a kinetic/Boltzmann scheme.

We can state the following result (see also [29])

THEOREM 4.1. *If we denote with $U^E(x, t + \Delta t)$ the solution of the Euler equations (2.7) with initial data $U^E(x, t) = \mathcal{P}(\beta(x, t)M_f(x, v, t))$ we have*

$$U^E(x, t + \Delta t) = U^K(x, t + \Delta t) + O(\Delta t^2). \quad (4.6)$$

Proof. In a time step Δt we can write for the Euler solution

$$U^E(x, t + \Delta t) = U^E(x, t) + \Delta t \partial_t U^E(x, t) + \frac{1}{2}(\Delta t)^2 \partial_{tt} U^E(x, t) + O(\Delta t^3)$$

and similarly

$$U^K(x, t + \Delta t) = U^K(x, t) + \Delta t \partial_t U^K(x, t) + \frac{1}{2}(\Delta t)^2 \partial_{tt} U^K(x, t) + O(\Delta t^3).$$

Clearly the zero order terms in the expansions are the same since the initial data of the Euler equations is simply the projection of the initial data for the transport equation

$$U^K(x, t) = \mathcal{P}(\beta(x, t)M_f(x, v, t)) = U^E(x, t).$$

Now let us consider the first order terms. We have

$$\partial_t U^E = -(\nabla_x \cdot (\rho u), \nabla_x \cdot (\rho u \otimes u + p), \nabla_x \cdot (Eu + pu))^T$$

and

$$\partial_t U^K = \mathcal{P}(-v \cdot \nabla_x f).$$

Note that this last equation is not closed since the right hand side involves third order moments of f . Again, however, the two terms evaluated at the initial time t coincide since the initial data for the transport step is the Maxwellian fraction $\beta(x, t)M_f(x, v, t)$ and so we have the usual Euler closure in the kinetic term. By similar arguments one can verify that the second order terms evaluated at the initial time are different because of the fourth order moments appearing in $\partial_{tt} U^K(x, t) = \mathcal{P}(v \cdot \nabla_x (v \cdot \nabla_x f))$. This proves (4.6).

□

By virtue of the above result we can replace the hybrid solution for the moments after the transport with

$$\tilde{U}^H(x, t + \Delta t) = U^P(x, t + \Delta t) + U^E(x, t + \Delta t), \quad (4.7)$$

without affecting the overall first order accuracy of the splitting method.

This hybrid values for the moments are used to compute the new Maxwellian $M_f^H(x, v, t + \Delta t)$ and advance the computation. To this goal we note that the next relaxation step takes the form

$$\begin{aligned} \mathcal{R}_{\Delta t}(\mathcal{T}_{\Delta t}(f(x, v, t))) &= \lambda \mathcal{T}_{\Delta t}(f(x, v, t)) + (1 - \lambda) M_f^H(x, v, t + \Delta t) \\ &= \lambda (\mathcal{T}_{\Delta t}((1 - \beta(x, t)) f^P(x, v, t)) + \mathcal{T}_{\Delta t}(\beta(x, t) M_f(x, v, t))) \\ &\quad + (1 - \lambda) M_f^H(x, v, t + \Delta t) \\ &= (1 - \beta(x, t + \Delta t)) f^P(x, v, t + \Delta t) + \beta(x, t + \Delta t) M_f^H(x, v, t + \Delta t), \end{aligned}$$

where we set

$$\beta(x, t + \Delta t) = 1 - \lambda, \quad f^P(x, v, t + \Delta t) = \mathcal{T}_{\Delta t}(f(x, v, t)) \quad (4.8)$$

with $\lambda = e^{-\Delta t/\varepsilon}$. This shows that in order to compute the new particle fraction we need to sample particles from $\mathcal{T}_{\Delta t}(\beta(x, t)M_f(x, v, t))$. In practice this can be realized in a simple way transforming initially the equilibrium Maxwellian part $\beta(x, t)M_f(x, v, t)$ into samples and then advecting the whole set of samples.

Let us denote with $\mathcal{T}_{\Delta t}(\beta(x, t)M_f^p(x, v, t))$ this set of advected equilibrium samples. Computationally this means that at each time step we must solve the full BGK model with a Monte Carlo scheme [12] together with a suitable deterministic solver for the Euler equation. We can improve the efficiency of the above algorithm observing that we do not need to transform into samples the whole Maxwellian part but only a fraction $\bar{\lambda}$ of it, where

$$\bar{\lambda} \geq \max_x \{\lambda(x, t + \Delta t)\}.$$

As discussed before, the reason for this is that we know that at the subsequent relaxation step a fraction $\beta(x, t + \Delta t)$ of samples will be discarded in each cell. Thus we need only

$$(1 - \beta(x, t + \Delta t))\mathcal{T}_{\Delta t}(\beta(x, t)M_f^p(x, v, t)) = \lambda(x, t + \Delta t)\mathcal{T}_{\Delta t}(\beta(x, t)M_f^p(x, v, t))$$

advected Maxwellian particles, which is guaranteed if in any cell before advection we have at least $\bar{\lambda}\beta(x, t)M_f^p(x, v, t)$ particles since

$$\mathcal{T}_{\Delta t}(\bar{\lambda}\beta(x, t)M_f^p(x, v, t)) = \bar{\lambda}\mathcal{T}_{\Delta t}(\beta(x, t)M_f^p(x, v, t)).$$

This is of paramount importance since $\bar{\lambda}$ vanishes as $\varepsilon/\Delta t \rightarrow 0$ and so the number of samples effectively used by the hybrid method is a decreasing function of the ration between the Knudsen number and the time step.

Starting from an initial data represented by particles a simple FSI hybrid scheme for the solution of the BGK equation with λ constant in space and time is described in the following algorithm

ALGORITHM 1 (FSI Hybrid Scheme).

1. Compute the initial velocity and position of the particles $\{\nu_j^0, j = 1, \dots, N\}$ $\{p_j^0, j = 1, \dots, N\}$ by sampling them from initial density $f_0(x, v)$. Set $m^p = \int \int f_0(x, v) dx dv / N$.
2. Given a mesh $x_i, i = 1, \dots, L$ with grid size Δx , and an estimate of the larger sample velocity $\nu_{max} = 4\sqrt{2T_{max}}$, with T_{max} the maximum temperature, set $\Delta t^p = \Delta x / \nu_{max}$.
3. Compute the initial values of the moments of the distribution function in each cell $q_i, (\rho u)_i, E_i, i = 1, \dots, L$.
4. Compute the larger time step allowed by the deterministic macroscopic scheme Δt_D .
5. Set $\Delta t = \min(\Delta t^p, \Delta t_D)$.
6. Set $n = 0, t = 0, \lambda = e^{-\Delta t/\varepsilon}, \bar{\lambda} = \lambda, \beta_i = 1 - \bar{\lambda}, i = 1, \dots, L$.
7. While $t \leq t_f$ with t_f the final chosen time.
 - (a) Estimate the number of Maxwellian samples we need from $\bar{\lambda}\beta(x, t)M_f^p(x, v, t)$.
 - i. In each cell set $N_i^M = \text{Iround}(\bar{\lambda}\beta_i \rho_i^n / (m^p / \Delta x))$ and sample N_i^M equilibrium particles from the Maxwellian with moments $(\rho u)_i^n, E_i^n$.
 - (b) Perform the transport step keeping track of the particles that come from the above sampling.
 - i. Transport all particles

$$p_j^{n+1} = p_j^n + \nu_j^n \Delta t, \quad \forall j. \quad (4.9)$$

- ii. Compute the moments $U_i^{p, n+1}$ and the number of particles N_i^p in each cell using only the advected particles not sampled from the Maxwellian.
- iii. Solve the Euler equations for $U_i^{E, n} = \beta_i U_i^n$ and find $U_i^{E, n+1}$.

- iv. Compute the new hybrid moments $U_i^{n+1} = U_i^{p,n+1} + U_i^{E,n+1}$
 - (c) Perform the relaxation step.
 - i. In each cell set $N_i^k = \text{Iround}(\lambda N_i^p)$ and discard $N_i^p - N_i^k$ particles.
 - ii. Compute the new number of particles in non equilibrium regime, in each cell $N_i^p = N_i^k + M_i^p$, $i = 1, \dots, L$, with M_i^p the transported Maxwellian particles (N_i^M transported).
 - iii. Compute the effective value $\lambda_i^p = (N_i^k + M_i^p)/(\varrho_i^{n+1} \Delta x / m^p)$.
 - iv. Set $\beta_i = 1 - \lambda_i^p$.
 - (d) Set $t = t + \Delta t$, $n = n + 1$ and compute the updated value of Δt .
- end while

REMARK 1.

- In this simple version of the FSI hybrid method the value of the equilibrium fraction fluctuates in each cell around the constant value $\beta = 1 - \lambda$, thus it depends on $\Delta t/\varepsilon$. We will see how to remove this limitation and make the equilibrium fraction essentially independent of Δt in the optimized version of the FSI scheme. Note that fluctuations are due to the fact that to have mass conservation during the relaxation step we compute the effective value λ_i^p and set $\beta_i = 1 - \lambda_i^p$.
- To avoid bias in the algorithm we used a stochastic rounding $\text{Iround}(x)$ of a positive real number x defined as

$$\text{Iround}(x) = \begin{cases} [x] & \text{with probability } [x] + 1 - x, \\ [x] + 1 & \text{with probability } x - [x], \end{cases}$$

where $[x]$ denotes the integer part of x .

- In the fluid limit the numerical method is characterized by the particular solver adopted to compute the solution of the Euler equation. Thus the order of accuracy of the limiting scheme is completely independent from the first order splitting procedure used to solve the kinetic equation. This is an advantage compared to the classical approach based on kinetic schemes which gives limited accuracy in time. Extensions to higher order in the non fluid regime are not trivial since we are limited to first order accuracy in time by Theorem 4.1.

4.1.1. Matching moments. In order to have a conservative scheme it is desirable that the set of advected equilibrium samples satisfies

$$\mathcal{P}(\mathcal{T}_{\Delta t}(\beta(x, t)M_f^p(x, v, t))) = U^E(x, t + \Delta t), \quad (4.10)$$

namely the kinetic particles solution to the fluid equations in one time step should match the direct solution to the limiting fluid equations. Moreover, since the right hand side is not affected by statistical sampling error, imposing (4.10) will decrease the variance of the samples.

To this goal it is natural to use a moment matching approach [3]. This can be done by simple transformations of the sample points. Given a set of samples ν_1, \dots, ν_J with first two moments μ_1 and μ_2 and a better estimate m_1 and m_2 of the same moments we can apply the transformation[3, 23]

$$\nu_j^* = (\nu_j - \mu_1)/c + m_1 \quad c = \sqrt{\frac{\mu_2 - \mu_1^2}{m_2 - m_1^2}}, \quad i = 1, \dots, J$$

to get

$$\frac{1}{J} \sum_{j=1}^J \nu_j^* = m_1, \quad \frac{1}{J} \sum_{j=1}^J (\nu_j^*)^2 = m_2.$$

Of course this renormalization is not possible for the mass density. In fact, to keep the algorithm simple, we take the weight of each particle m^p equal and constant during the simulation and this implies that we can have only integer multiples of such weights as mass density values in each cell.

However thanks to the particular structure of the algorithm we can perform also a matching procedure for the mass using the following trick. After the transport of Maxwellian particles we need in each cell, in order to perform the moment matching of order zero, a number of particles given by

$$M_i^p = \text{Iround}(\lambda \rho^E(x_i, t + \Delta t)/m^p).$$

This can be done if we take $\bar{\lambda}$ large enough before transport which guarantees that we have enough particles in each cell. In this way the difference between the particles mass and the Euler mass is below the mass of one single particle.

Next, to have exactly mass conservation we compute the effective values

$$\lambda_i^p = (M_i^p + N_i^k)/(\rho^E(x_i, t + \Delta t)\Delta x/m^p + N_i^p), \quad \beta^p(x_i, t + \Delta t) = 1 - \lambda_i^p,$$

used in the method. After this we renormalize the transported equilibrium samples in each space cell as described above so that they have the same momentum and energy of the Euler solution.

Similarly one can apply a moment matching strategy when sampling from the Maxwellian during the relaxation step. In this case, as an alternative to the moment matching technique described above, one can use the algorithm developed by Pullin [30].

Note that the whole method can be seen as a Monte Carlo scheme for the BGK equation in which we try to reduce fluctuations substituting the moments of the transported Maxwellian, computed with particles, with the moments given by the solution of the compressible Euler equation obtained with a deterministic macroscopic scheme. Moreover, as described above, if we force the equilibrium particles to follow the moments given by the fluid equations we can reinterpret the algorithm as a fluid-dynamic guided Monte Carlo scheme.

4.2. Optimal FSI Methods. The method just described does not take into account the possibility to optimize the equilibrium fraction by increasing its value in time and make it independent on the choice of the time step. In fact at each time step the equilibrium structure is entirely lost and the new fraction of equilibrium is only given by the relaxation step (see 4.8). However, in principle, it is possible to recover some information from the transported local Maxwellian although we know it through samples rather than analytically. We recall, in fact, that we do not get any microscopic information from $U^E(x, t)$ which corresponds to the solution of the Euler equation with a macroscopic numerical scheme. In the sequel, we will propose a method to optimize the equilibrium fraction $\beta(x, t)$ after the transport step. We start describing the generalization of the hybrid method once this optimization has been achieved.

Thanks to Definition 1 we can define the velocity dependent optimal equilibrium fraction as the ratio of the transported Maxwellian at time t respect to the new local Maxwellian at time $n + 1$

$$w^c(x, v, t + \Delta t) = \begin{cases} \frac{\mathcal{T}_{\Delta t}(\beta(x, t)M_f(x, v, t))}{M_f^H(x, v, t + \Delta t)}, & \mathcal{T}_{\Delta t}(\beta(x, t)M_f(x, v, t)) \leq M_f^H(x, v, t + \Delta t), \\ 1, & \mathcal{T}_{\Delta t}(\beta(x, t)M_f(x, v, t)) \geq M_f^H(x, v, t + \Delta t), \end{cases}$$

and the optimal equilibrium fraction as

$$\beta^c(x, t + \Delta t) = \min_v \{w^c(x, v, t + \Delta t)\}. \quad (4.11)$$

This value can be considered optimal, in the sense that it is the maximum allowed value for which we have a decomposition like

$$\mathcal{T}_{\Delta t}(\beta(x, t)M_f(x, v, t)) = \tilde{M}_f(x, v, t + \Delta t) + \beta^c(x, t + \Delta t)M_f^H(x, v, t + \Delta t) \quad (4.12)$$

with $\tilde{M}_f(x, v, t + \Delta t) \geq 0$. Clearly similar decompositions hold true for any fraction of equilibrium below the optimal one.

Suppose, for simplicity, that $\beta^c(x, t) = 0$ at the beginning of our computation, it follows that the method reads in the same way from equation (4.4) to equation (4.7). Now, given an estimation for $\beta^c(x, t + \Delta t)$ the next relaxation step reads as

$$\begin{aligned}
\mathcal{R}_{\Delta t}(\mathcal{T}_{\Delta t}(f(x, v, t))) &= \lambda \mathcal{T}_{\Delta t}(f(x, v, t)) + (1 - \lambda) M_f^H(x, v, t + \Delta t) \\
&= \lambda(\mathcal{T}_{\Delta t}((1 - \beta(x, t))f^p(x, v, t)) + \mathcal{T}_{\Delta t}(\beta(x, t)M_f(x, v, t))) \\
&\quad + (1 - \lambda) M_f^H(x, v, t + \Delta t) \\
&= \lambda(\mathcal{T}_{\Delta t}((1 - \beta(x, t))f^p(x, v, t)) + \beta^c(x, t + \Delta t)M_f^H(x, v, t + \Delta t) \\
&\quad + \tilde{M}_f(x, v, t + \Delta t)) + (1 - \lambda) M_f^H(x, v, t + \Delta t) \\
&= (1 - \beta(x, t + \Delta t))f^p(x, v, t + \Delta t) + \beta(x, t + \Delta t)M_f^H(x, v, t + \Delta t),
\end{aligned}$$

with

$$\beta(x, t + \Delta t) = 1 - \lambda(1 - \beta^c(x, t + \Delta t)) \quad (4.13)$$

and

$$f^p(x, v, t + \Delta t) = \frac{\mathcal{T}_{\Delta t}((1 - \beta(x, t))f^p(x, v, t)) + \tilde{M}_f(x, v, t + \Delta t)}{1 - \beta^c(x, t + \Delta t)}. \quad (4.14)$$

In order to sample from the distribution $\tilde{M}_f(x, v, t + \Delta t)$, which is obtained as a difference of two distribution functions, see (4.12), we can sample particles, exactly as in the previous section, from the transported Maxwellian and then apply an acceptance rejection technique that reads

ALGORITHM 2 (Acceptance-Rejection Sampling).

do $i = 1, N$ with N number of particles to be sampled

1. Select randomly one particle from the distribution $\mathcal{T}_{\Delta t}(\beta(x, t)M_f(x, v, t))$;
2. with probability $1 - \frac{\beta^c(x, t + \Delta t)M_f^H(x, v, t + \Delta t)}{\mathcal{T}_{\Delta t}(\beta(x, t)M_f(x, v, t))}$ keep the particle.

In the above algorithm particles can be taken more than once, in other words the sampling is not exclusive. Finally a moment matching strategy similar to the one described in the previous section can be used in such a way that the equation

$$\mathcal{P}(\tilde{M}_f(x, v, t + \Delta t)) = U^E(x, t + \Delta t) - \beta^c(x, t + \Delta t)\tilde{U}^H(x, t + \Delta t), \quad (4.15)$$

is satisfied exactly.

The major problem we have to face when practically evaluating $\beta^c(x, t + \Delta t)$ is that $M_f^H(x, v, t + \Delta t)$ is known analytically while $\mathcal{T}_{\Delta t}(\beta(x, t)M_f(x, v, t))$ is known only through samples. From a numerical viewpoint when approximating $\beta^c(x, t + \Delta t)$ we want to avoid overestimates since these may produce unphysical solutions. In the following description, to simplify notations, we restrict to 1-D in velocity and physical space, extensions of the methods to multidimensional cases are straightforward. Our goal is to find an estimation of $\beta^c(x, t)$ given by (4.11). Without loss of generality we assume that at each point x there exist a velocity v such that

$$\mathcal{T}_{\Delta t}(\beta(x, t)M_f(x, v, t)) \leq M_f^H(x, v, t + \Delta t).$$

In fact, for those space points x where the above assumption is not satisfied we simply have $\beta^c(x, t + \Delta t) = 1$.

The first and simplest method consists in measuring the departure from equilibrium reconstructing the transported Maxwellian from samples. In order to do that we need a grid in velocity space and a loop over the particles inside each spatial cell. We omit here the details of the different reconstruction methods that can be used, we refer to [26] (and the references therein) for the technical aspects.

Once we have reconstructed $\mathcal{T}_{\Delta t}(\beta(x_i, t)M_f(x_i, v, t))$, with $\{x_i\}_{i \in I}$ a mesh of the physical space, we are able to determine the quantity

$$\beta^c(x_i, t + \Delta t) = \min_v \left\{ \frac{\mathcal{T}_{\Delta t}(\beta(x_i, t)M_f(x_i, v, t))}{M_f^H(x_i, v, t + \Delta t)} \right\}. \quad (4.16)$$

This method presents several drawbacks. The reconstruction of the distribution function from samples increase the computational cost, moreover a small number of particles inside a cell, which is quite common in applications, gives large fluctuations and this turns in an imprecise estimate of $\beta^c(x, t)$.

A better way to estimate the equilibrium fraction $\beta^c(x, t)$ after the transport is based on the analysis of a deterministic transport of the Maxwellian part. Again we introduce a grid in space. We consider the following scheme for the transport of the Maxwellian fraction

$$\frac{\hat{M}_{f,i}^{n+1}(v) - M_{f,i}^n(v)}{\Delta t} + v \frac{M_{f,i}^n(v) - M_{f,i-1}^n(v)}{\Delta x} = 0, \quad v \geq 0, \quad (4.17)$$

$$\frac{\hat{M}_{f,i}(v)^{n+1} - M_{f,i}^n(v)}{\Delta t} + v \frac{M_{f,i+1}^n(v) - M_{f,i}^n(v)}{\Delta x} = 0, \quad v < 0,$$

where $M_{f,i}^n(v) \approx M_f(x_i, v, t^n)$, $\hat{M}_{f,i}^{n+1}(v) \approx M_f(x_i, v, t^{n+1})$ and Δx is the mesh size in space. We put an hat on the transported Maxwellian to distinguish it with respect to the local Maxwellian at time $t + \Delta t$, which is accordingly to the notations, $M_{f,i}^{n+1}(v)$. The scheme described above is a simple first order upwind for the Maxwellian transport. Of course to effectively perform the computation it is necessary to truncate the Maxwellian in order to obtain finite values for the velocity and time step larger than zero. Typically this truncation leads to several problems which are common in numerical methods for kinetic equations (see for example [18, 25]). Here we are only interested to estimate the departure from the equilibrium of the transported Maxwellian and for that scope we choose a bound for the velocity space in such a way that no additional time step restrictions are imposed. Solving Eqs. (4.18) we obtain

$$\hat{M}_{f,i}^{n+1}(v) = \left(1 - \frac{v\Delta t}{\Delta x}\right) M_{f,i}^n(v) + \frac{v\Delta t}{\Delta x} M_{f,i-1}^n(v), \quad v \geq 0, \quad (4.18)$$

$$\hat{M}_{f,i}^{n+1}(v) = \left(1 + \frac{v\Delta t}{\Delta x}\right) M_{f,i}^n(v) - \frac{v\Delta t}{\Delta x} M_{f,i+1}^n(v), \quad v < 0.$$

Note that, since $|v|\Delta t \leq \Delta x$, the updated function $\hat{M}_{f,i}^{n+1}(v)$ is a convex combination of the local Maxwellian in the cells i and $i - 1$ for positive velocities and in the cells i and $i + 1$ for negative velocities.

Now, ignoring the error introduced by the truncation in velocity, in each cell the equilibrium fraction $\beta^c(x_i, t + \Delta t)$ satisfies

$$\beta^c(x_i, t + \Delta t) = \min_v \left\{ \frac{\mathcal{T}_{\Delta t}(\beta(x_i, t)M_f(x_i, v, t))}{M_f^H(x_i, v, t + \Delta t)} \right\} = \min_v \left\{ \frac{\hat{M}_{f,i}^{n+1}(v)}{M_{f,i}^{H,n+1}(v)} \right\} + O(\Delta t^2). \quad (4.19)$$

In the general case a numerical method is required to compute the minimum on the right hand side. This operation can be expensive since it has to be done at each time step and in each spatial cell. However we can restrict ourselves to a lower estimate of $\beta^c(x_i, t + \Delta t)$ (to avoid an overestimate of the equilibrium fraction) and we can choose instead of the minimum a lower bound for (4.19) using the convexity property of the scheme. That value can be estimated observing that

$$\begin{aligned} \min_{v \geq 0} \left\{ \frac{\hat{M}_{f,i}^{n+1}(v)}{M_{f,i}^{H,n+1}(v)} \right\} &\geq \min \left\{ \min_{v \geq 0} \left\{ \frac{M_{f,i}^n(v)}{M_{f,i}^{H,n+1}(v)} \right\}, \min_{v \geq 0} \left\{ \frac{M_{f,i-1}^n(v)}{M_{f,i}^{H,n+1}(v)} \right\} \right\} \\ &= \beta_R^c(x, t + \Delta t), \end{aligned} \quad (4.20)$$

$$\begin{aligned} \min_{v < 0} \left\{ \frac{\hat{M}_{f,i}^{n+1}(v)}{M_{f,i}^{H,n+1}(v)} \right\} &\geq \min \left\{ \min_{v < 0} \left\{ \frac{M_{f,i}^n(v)}{M_{f,i}^{H,n+1}(v)} \right\}, \min_{v < 0} \left\{ \frac{M_{f,i+1}^n(v)}{M_{f,i}^{H,n+1}(v)} \right\} \right\} \\ &= \beta_L^c(x, t + \Delta t), \end{aligned} \quad (4.21)$$

and setting

$$\beta^c(x, t + \Delta t) = \min\{\beta_R^c(x, t + \Delta t), \beta_L^c(x, t + \Delta t)\} \quad (4.22)$$

where the minimum of the ratios in (4.20)-(4.21) can be computed exactly, being the ratios of Maxwellian functions.

An algorithm that can be used to implement the optimized FSI method for the solution of the BGK equation, in which for simplicity λ is constant, is the following

ALGORITHM 3 (Optimized FSI Hybrid Scheme).

1. Compute the initial velocity and position of the particles $\{\nu_j^0, j = 1, \dots, N\}$ $\{p_j^0, j = 1, \dots, N\}$ by sampling them from initial density $f_0(x, v)$. Set $m^p = \int \int f_0(x, v) dx dv / N$.
2. Given a mesh $x_i, i = 1, \dots, L$ with grid size Δx , and an estimate of the larger sample velocity $\nu_{max} = 4\sqrt{2T_{max}}$, with T_{max} the maximum temperature, set $\Delta t^p = \Delta x / \nu_{max}$.
3. Compute the initial values of the moments of the distribution function in each cell $\rho_i, (\rho u)_i, E_i, i = 1, \dots, L$.
4. Compute the larger time step allowed by the deterministic macroscopic scheme Δt_D .
5. Set $\Delta t = \min(\Delta t^p, \Delta t_D)$.
6. Set $n = 0, t = 0, \lambda = e^{-\Delta t/\varepsilon}, \bar{\lambda} = \lambda, \beta_i = 1 - \bar{\lambda}, i = 1, \dots, L$.
7. While $t \leq t_f$ with t_f the final chosen time.

- (a) Estimate the number of Maxwellian samples we need from $\bar{\lambda}\beta(x, t)M_f^p(x, v, t)$.
 - i. In each cell set $N_i^M = \text{Iround}(\beta_i \rho_i^n / (m^p / \Delta x))$ and sample N_i^M equilibrium particles from the Maxwellian with moments $(\rho u)_i^n, E_i^n$.
- (b) Perform the transport step keeping track of the particles that come from the above sampling.
 - i. Transport all particles

$$p_j^{n+1} = p_j^n + \nu_j^n \Delta t, \quad \forall j. \quad (4.23)$$

- ii. Compute the moments $U_i^{p,n+1}$ and the number of particles N_i^p in each cell using only the advected particles not sampled from the Maxwellian.
- iii. Solve the Euler equations for $U_i^{E,n} = \beta_i U_i^n$ and find $U_i^{E,n+1}$.
- iv. Compute the new hybrid moments $U_i^{n+1} = U_i^{p,n+1} + U_i^{E,n+1}$
- (c) Compute the optimal equilibrium fraction $\beta_i^{c,n+1}$ as described in (4.20)-(4.22).

- (d) *Perform the relaxation step.*
- i. In each cell set $N_i^k = \text{Iround}(\lambda N_i^p)$ and discard $N_i^p - N_i^k$ particles.*
 - ii. In each cell sample \tilde{N}_i^M particles from the distribution $\tilde{M}_{f,i}^{n+1}(v)$ with the acceptance-rejection technique described in Algorithm 2.*
 - iii. Apply the moment matching technique to the \tilde{N}_i^M particles in order to satisfy (4.15).*
 - iv. Compute the new number of particles in non equilibrium regime, in each cell $N_i^p = N_i^k + \tilde{N}_i^M$, $i = 1, \dots, L$.*
 - v. Compute the effective equilibrium fraction $\beta_i = 1 - (N_i^k + \tilde{N}_i^M)/(\varrho_i^{n+1} \Delta x / m^p)$.*
- (e) *Set $t = t + \Delta t$, $n = n + 1$ and compute the updated value of Δt .*
end while

REMARK 2.

- We emphasize that the first order upwind method to compute the deterministic transport of Maxwellians is never used in practice. It serves us only as an approximation strategy in order to compute a lower bound for the optimal equilibrium fraction $\beta^c(x, t + \Delta t)$. In this sense it is worth to notice that the additional first order dissipation introduced by this upwinding produces additional smearing and in principle, close to discontinuities, can produce overestimates of the equilibrium fraction when computed from (4.19). Besides computational efficiency this is an additional motivation to use a lower bound for that value.
- The hybrid composition of the solution in the final method does not depend on the time step Δt but only on ε . Note, however, that small time steps, below the CFL condition of the deterministic Euler solver, may increase the computational cost. To reduce this effect one can use different time steps in the kinetic and the Euler solver and perform the hybridization and matching only at intermediate steps. This strategy can be used, for example, where there is the need to resolve small scales at the Navier-Stokes level or in boundary layer effects.

5. Implementation and numerical tests. In principle any finite volume or finite difference numerical scheme can be used to solve the compressible Euler equations in our hybrid method. In the sequel we will use a second order finite volume MUSCL type relaxed scheme (see [17] for details).

In the next paragraphs we analyze the performances of the fluid solver independent hybrid schemes in comparison with a classical Monte Carlo method (MCM) for several one-dimensional problems with different Knudsen numbers ranging from $\varepsilon = 10^{-2}$ to $\varepsilon = 10^{-5}$.

As a reference solution we used a deterministic discrete velocity model (DVM) for the BGK equation for all tests (see [18] for details). We use the shorthand FSI, FSI1 and TVD to denote the simple FSI method, the optimal FSI method and the second order in space MUSCL Euler solver respectively.

5.1. Accuracy test. Because our aim is to compare the differences in accuracy and computational time between the different methods first we have considered an accuracy test with a periodic smooth solution. We compare the results of the kinetic-solver based hybrid methods developed in [12] to the new independent fluid solver schemes.

We report the total L_1 norm of the errors for the conserved quantity ϱ , u , and T as the computational times by considering a problem with the following initial data

$$\begin{aligned} \varrho(x, 0) &= 1 + a_\varrho \sin \frac{2\pi x}{L} \\ u(x, 0) &= 1.5 + a_u \sin \frac{2\pi x}{L} \end{aligned} \tag{5.1}$$

	$\varepsilon = 10^{-2}$	$\varepsilon = 10^{-3}$	$\varepsilon = 10^{-4}$	$\varepsilon = 10^{-5}$
MCM N=1500	23 sec	25 sec	27 sec	26 sec
BHM N=1500	35 sec	25 sec	22 sec	22 sec
BHM1 N=1500	34 sec	20 sec	19 sec	20 sec
BCHM N=1500	15 sec	11 sec	17 sec	21 sec
FSI N=1500	25 sec	22 sec	3 sec	0.6 sec
FSI1 N=1500	18 sec	17 sec	2 sec	0.6 sec
FSI N=500	9 sec	8 sec	0.4 sec	0.3 sec
FSI1 N=500	7 sec	6 sec	0.4 sec	0.3 sec

TABLE 5.1

Accuracy test. Computational times for FSI and FSI1 with two different initial numbers of particles $N = 1500$ and $N_1 = 500$ compared to the previous hybrid methods (see [12]) for different values of the Knudsen number.

	$\varepsilon = 10^{-2}$	$\varepsilon = 10^{-3}$	$\varepsilon = 5 \times 10^{-4}$	$\varepsilon = 10^{-4}$
MCM	5.494	5.786	5.153	5.184
FSI	5.545	3.926	3.067	0.268
FSI1	4.588	3.406	2.451	0.243

TABLE 5.2

Accuracy test. L_1 norm of the error (in units of 10^{-2}) for the density with respect to different values of the Knudsen number ε .

$$E(x, 0) = 2.5 + a_T \sin \frac{2\pi x}{L}$$

where we set

$$a_\rho = 0.3 \quad a_u = 0.1 \quad a_E = 1.$$

The equations are integrated for $t \in [0, 5 \times 10^{-2}]$ using 200 space cell.

In order to make a fair comparison with the previous schemes named BHM, BHM1, BCHM (see [12] for details and parameters settings of the methods) we use at the beginning 1500 particles for cell with the same time step of the Boltzmann-BGK schemes. Then, because in general FSI type schemes allow larger time steps and the moment matching techniques produce lower fluctuations we repeat the computation with $N = 500$ and the time step prescribed by the Monte Carlo method. We remark that, while estimating the time differences between the FSI schemes and MCM is quite easy (in fact the FSI methods are based on the MCM for the kinetic part), the same comparison with another kinetic solver such as DVM or BHM, is not straightforward due to the several possible choices involved in such schemes (for example the way the velocity domain is truncated and the type of solver chosen for the space derivatives). For this reason we stress that the simulations times, reported in Table 1, are just indicative. It is clear that the hybrid methods here developed represent a strong improvement with respect to the previous schemes as well as to the classical Monte Carlo method in terms of computational time. In Figure 5.1 we report the total number of particles used by the different algorithms. Note how computational time and fluctuations reduce dramatically when the Knudsen number diminishes.

The results for the relative L_1 errors are reported in Tables 5.2, 5.3, 5.4, respectively for density, mean velocity and temperature for the FSI, FSI1 and the Monte Carlo schemes. In all the methods we used $N = 200$ particles for cell and the moment matching techniques. We notice that the hybrid methods have approximately the same accuracy of the Euler solver for small Knudsen numbers and the same accuracy of the Monte Carlo method for large Knudsen while to intermediate values correspond intermediate behaviors. From the above results it is clear how the performances of

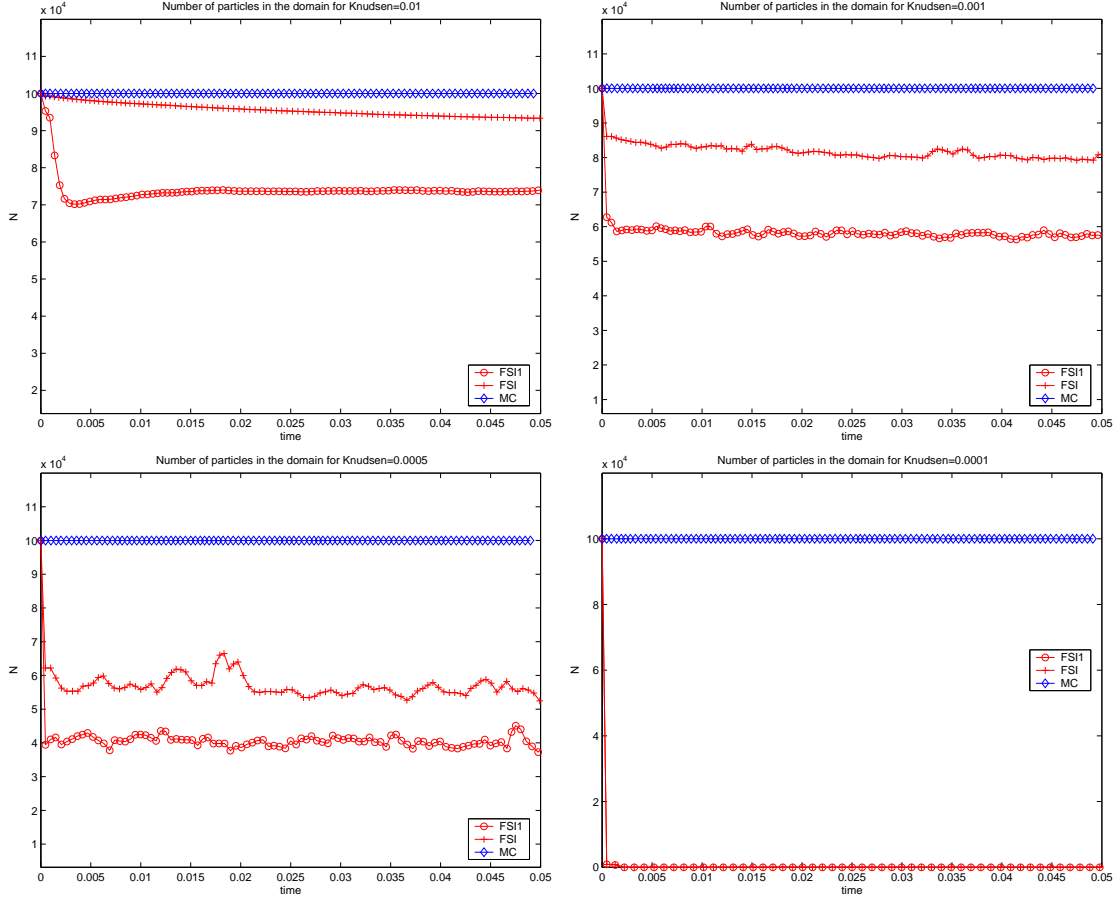


FIG. 5.1. Accuracy test. Number of particles in time inside the computational domain for FSI1, FSI and MC schemes. Knudsen numbers $\varepsilon = 10^{-2}$ (top left) $\varepsilon = 10^{-3}$ (top right) $\varepsilon = 5 \times 10^{-4}$ (bottom left) and $\varepsilon = 10^{-4}$ (bottom right).

	$\varepsilon = 10^{-2}$	$\varepsilon = 10^{-3}$	$\varepsilon = 5 \times 10^{-4}$	$\varepsilon = 10^{-4}$
MCM	6.565	5.437	5.338	6.035
FSI	4.802	4.401	3.264	0.641
FSI1	5.135	4.102	2.848	0.610

TABLE 5.3

Accuracy test. L_1 norm of the error (in units of 10^{-2}) for the mean velocity with respect to different values of the Knudsen number ε .

the hybrid schemes are better than the ones of a Monte Carlo method, moreover FSI1 gives in general better results respect to FSI both in term of computational time and accuracy for almost all regimes.

5.2. 1-D Unsteady shock. Next we consider an unsteady shock that propagates from left to right. The shock is produced miming a specular wall on the left boundary, thus for the stochastic component at each time step, particles which escape from the computational domain on the left side are put back in the first cell with opposite velocity and opposite position respect to zero. On

	$\varepsilon = 10^{-2}$	$\varepsilon = 10^{-3}$	$\varepsilon = 5 \times 10^{-4}$	$\varepsilon = 10^{-4}$
MCM	6.762	7.611	7.578	7.316
FSI	7.007	6.022	4.500	0.641
FSI1	6.662	4.939	3.773	0.598

TABLE 5.4

Accuracy test. L_1 norm of the error (in units of 10^{-2}) for the temperature with respect to different values of the Knudsen number ε .

the other side particles are injected with the initial mean velocity and temperature in a number which corresponds to the initial density. For the macroscopic part the usual specular and inflow boundary condition are used. At the beginning the flow is uniform with mass $\varrho = 1$, mean velocity $u = -1$ and energy $E = 2.5$. The computations are stopped when $t = 0.065$, the number of cells are 200 in space, while the initial number of particle are 500 for each space cell. In each Figure the solution computed with the Euler scheme and the one computed with the DVM scheme is reported. The FSI, FSI1 and MCM are respectively depicted for density, mean velocity and temperature. We observe that for large Knudsen numbers FSI (Figure 5.2 left) and FSI1 (Figure 5.2 right) provide a small improvement with respect to MCM (Figure 5.6 left) in term of fluctuations. When ε decreases the non-equilibrium part becomes smaller and both FSI and FSI1 (Figure 5.3 and 5.4) contain less fluctuations than MCM. Note that, since the time step here is $O(\varepsilon)$, the reduction of fluctuations in FSI scheme is essentially the same for $\varepsilon = 0.001$ and $\varepsilon = 0.0005$ whereas for FSI1 scheme the solution shows a remarkable improvement as ε diminishes. Finally for $\varepsilon = 10^{-4}$ (Figure 5.5) we are in an under-resolved regime and both hybrid methods yield similar solutions at the same computational time.

5.3. 1-D Lax Shock Tube Test. Finally we consider a Lax shock tube test with initial values

$$\mathbf{u}_L = \begin{pmatrix} 0.445 \\ 0.598 \\ 3.5 \end{pmatrix}, \text{ if } 0 \leq x < 0.5 \quad \mathbf{u}_R = \begin{pmatrix} 0.5 \\ 0 \\ 0.48 \end{pmatrix}, \text{ if } 0.5 \leq x \leq 1.$$

The solution is computed with 200 grid points in space, the final time is $t = 0.05$. The initial number of particle is 500 for each space cell. Each Figure contains the DVM solution and the Euler solution as reference. Similar considerations to those of the previous section hold for this test case. Thus for large Knudsen numbers the solutions computed with the hybrid methods (Figure 5.8-5.9) show small improvements compared to the Monte Carlo scheme (Figure 5.12). On the other hand when the Knudsen number becomes smaller FSI and FSI1 schemes (Figure 5.10-5.11) give a considerable reduction of fluctuations. This is especially true for FSI1 method which demonstrates the importance of a good estimate of the equilibrium fraction β^c after the transport.

6. Conclusion. In this paper we have extended the hybrid kinetic methods developed in [12] to the case of an arbitrary fluid solver for the equilibrium component. Although, the simplified BGK collision operator has been used to develop the schemes, extensions to the full Boltzmann operator of rarefied gas dynamics in principle are possible through the use of time relaxed methods [21, 24]. We plan to extend the schemes to the full Boltzmann equation in the nearby future.

The results obtained are very promising in terms of computational cost with respect to traditional deterministic methods for kinetic equations like discrete velocity model or spectral schemes [18, 25]. In addition the FSI hybrid algorithms yield less fluctuations with respect to direct simulation Monte Carlo methods and, close to the fluid regime, they permit to compute results faster. A remarkable feature of the FSI1 scheme is that the equilibrium fraction is essentially independent

of the choice of the time step and thus provides more accurate results than Monte Carlo methods even in resolved regimes.

Some open questions remain on alternative ways to estimate and increase the fraction of equilibrium in each space cell without increasing the computational cost. It is also interesting, and will be the subject of future works, to measure the response of the FSI hybrid methods in other situations such as simulations of nanosystem devices, plasma physics problems or turbulence.

Acknowledgements. The authors would like to thank Russ Caflisch and Pierre Degond for several stimulating discussions.

REFERENCES

- [1] G.A.BIRD, *Molecular gas dynamics and direct simulation of gas flows*, Clarendon Press, Oxford (1994).
- [2] J. F. BOURGAT, P. LETALLEC, B. PERTHAME, AND Y. QIU, *Coupling Boltzmann and Euler equations without overlapping*, in Domain Decomposition Methods in Science and Engineering, Contemp. Math. 157, AMS, Providence, RI, (1994), pp. 377–398.
- [3] R. E. CAFLISCH, *Monte Carlo and Quasi-Monte Carlo Methods*, Acta Numerica (1998) pp. 1–49.
- [4] C. CERCIGNANI, *The Boltzmann Equation and Its Applications*, Springer-Verlag, New York, (1988).
- [5] C. CERCIGNANI, *Rarefied Gas Dynamics: From Basic Concepts to Actual Calculations*, Cambridge Texts in Applied Mathematics, Cambridge University Press, Cambridge (2000).
- [6] F. CORON, B. PERTHAME, *Numerical passage from kinetic to fluid equations*, SIAM J. Numer. Anal., vol. 28 (1991), pp. 26–42.
- [7] N. CROUSEILLES, P. DEGOND, M. LEMOU, *A hybrid kinetic-fluid model for solving the gas-dynamics Boltzmann BGK equation*, Journal of Computational Physics, vol. 199 (2004), pp. 776–808.
- [8] S. DESHPANDE, *A second order accurate kinetic theory based method for inviscid compressible flow*. Journal of Computational Physics, (1979).
- [9] P. DEGOND, G. DIMARCO, L. MIEUSSENS, *A moving interface method for dynamic kinetic-fluid coupling*, Journal of Computational Physics Vol. 227, pp. 1176–1208.
- [10] P. DEGOND, S. JIN, L. MIEUSSENS, *A Smooth Transition Between Kinetic and Hydrodynamic Equations*, Journal of Computational Physics, vol. 209 (2005), pp. 665–694.
- [11] G. DIMARCO, L. PARESCHI, *Hybrid multiscale methods I. Hyperbolic Relaxation Problems*, Comm. Math. Sci., 1, (2006), pp. 155–177.
- [12] G. DIMARCO, L. PARESCHI, *Hybrid multiscale methods II. Kinetic equations*, SIAM Multiscale Modeling and Simulation Vol 6., No 4, pp. 1169–1197, (2008).
- [13] G. DIMARCO, L. PARESCHI, *Domain decomposition techniques and hybrid multiscale methods for kinetic equations*, Proceedings of the 11th International Conference on Hyperbolic problems: Theory, Numerics, Applications, pp. 457–464.
- [14] W. E, B. ENGQUIST, *The heterogeneous multiscale methods*, Comm. Math. Sci., vol. 1 (2003), pp. 87–133.
- [15] W. E, B. ENGQUIST, *Multiscale Modeling and Computation*, Notices of the AMS, vol. 50(9) (2003), pp. 1062–1070.
- [16] S. JIN, *Runge-Kutta methods for hyperbolic conservation laws with stiff relaxation terms*, J. Comput. Phys., 122 (1995), pp. 51–67.
- [17] S. JIN, Z. P. XIN, *Relaxation schemes for systems of conservation laws in arbitrary space dimensions*, Comm. Pure Appl. Math., vol. 48 (1995), pp. 235–276.
- [18] L. MIEUSSENS, *Discrete Velocity Model and Implicit Scheme for the BGK Equation of Rarefied Gas Dynamic*, Mathematical Models and Methods in Applied Sciences, Vol. 10 No. 8 (2000), 1121–1149
- [19] P. LETALLEC, F. MALLINGER, *Coupling Boltzmann and Navier-Stokes by half fluxes* Journal of Computational Physics, vol. 136 (1997), pp. 51–67.
- [20] S. LIU, *Monte Carlo strategies in scientific computing*, Springer, (2004).
- [21] L. PARESCHI, R. E. CAFLISCH, *Implicit Monte Carlo methods for rarefied gas dynamics I: The space homogeneous case*, J. Comput. Phys., vol. 154 (1999), pp. 90–116.

- [22] L. PARESCHI, R. E. CAFLISCH, *Towards an hybrid method for rarefied gas dynamics*, IMA Vol. App. Math., vol. 135 (2004), pp. 57–73.
- [23] L. PARESCHI, S. TRAZZI, *Numerical Solution of the Boltzmann equation by time relaxed Monte Carlo (TRMC) methods*, International Journal for Numerical Methods in Fluids, vol. 48 (2005), pp. 947-983.
- [24] L. PARESCHI, G. RUSSO, *Time Relaxed Monte Carlo methods for the Boltzmann equation*, SIAM J. Sci. Comput. 23 (2001), pp. 1253–1273.
- [25] L. PARESCHI, G. RUSSO, *Numerical solution of the Boltzmann equation. I. Spectrally accurate approximation of the collision operator*. SIAM J. Numer. Anal. 37 (2000), no. 4, 1217–1245.
- [26] L. PARESCHI, *Hybrid multiscale methods for hyperbolic and kinetic problems*, Esaim Proceedings, Vol. 15, T. Goudon, E. Sonnendruker & D. Talay Editors, pp.87-120, (2005).
- [27] S. PIERACCINI, G. PUPPO, *Implicit-explicit schemes for BGK kinetic equations*, Journal of Scientific Computing, Volume 32, Number 1, July 2007 , pp. 1–28.
- [28] B. PERTHAME, *Boltzmann type schemes for gas dynamics and the entropy property*, SIAM J. Num. Anal., Vol. 27, (1990), pp. 1405.
- [29] B. PERTHAME, *Second-Order Boltzmann Schemes for Compressible Euler Equations in One and Two Space Dimensions*, SIAM J. Num. Anal., Vol. 29, No. 1, (1992), pp. 1-19.
- [30] D. I. PULLIN, *Generation of normal variates with given sample*, J. Statist. Comput. Simulation, 9 (1979), pp. 303–309.
- [31] R. ROVEDA, D.B. GOLDSTEIN, P.L. VARGHESE, *Hybrid Euler/Direct Simulation Monte Carlo Calculation of Unsteady Slit Flow*, AIAA J. Spacecraft Rockets, vol. 37 (2000), pp. 753-760.
- [32] S. TIWARI, *Coupling of the Boltzmann and Euler equations with automatic domain decomposition*, J. Comput. Phys., vol. 144, 1998, 710–726.
- [33] K. XU, *A gas-kinetic BGK scheme for the Navier-Stokes equations and its connection with artificial dissipation and Godunov method*. J. Comput. Phys. 171 (2001), no. 1, 289–335.

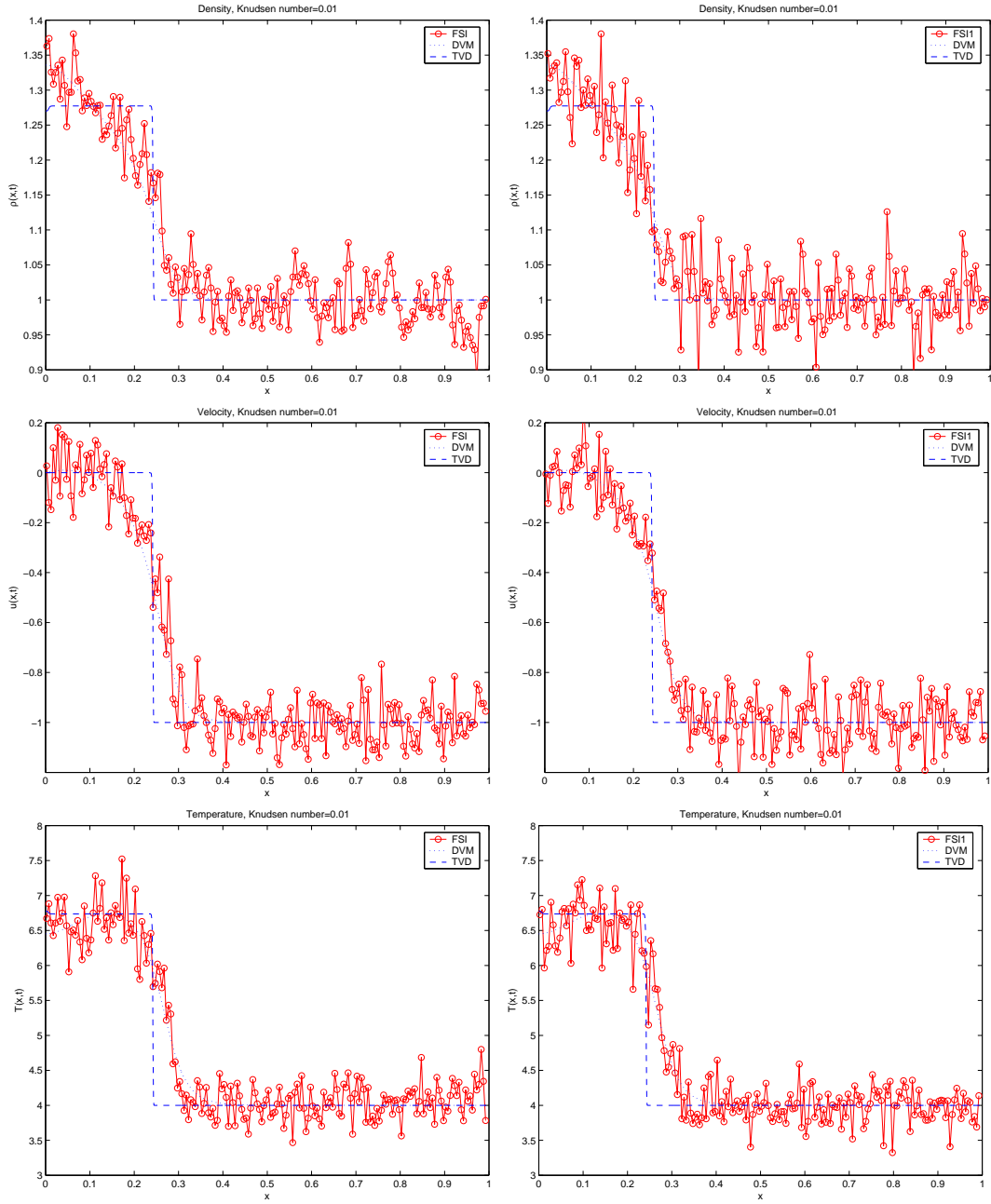


FIG. 5.2. Unsteady Shock: $\varepsilon = 10^{-2}$. Solution at $t = 0.065$ for FSI (left) FSI1 (right). From top to bottom density, mean velocity and temperature.

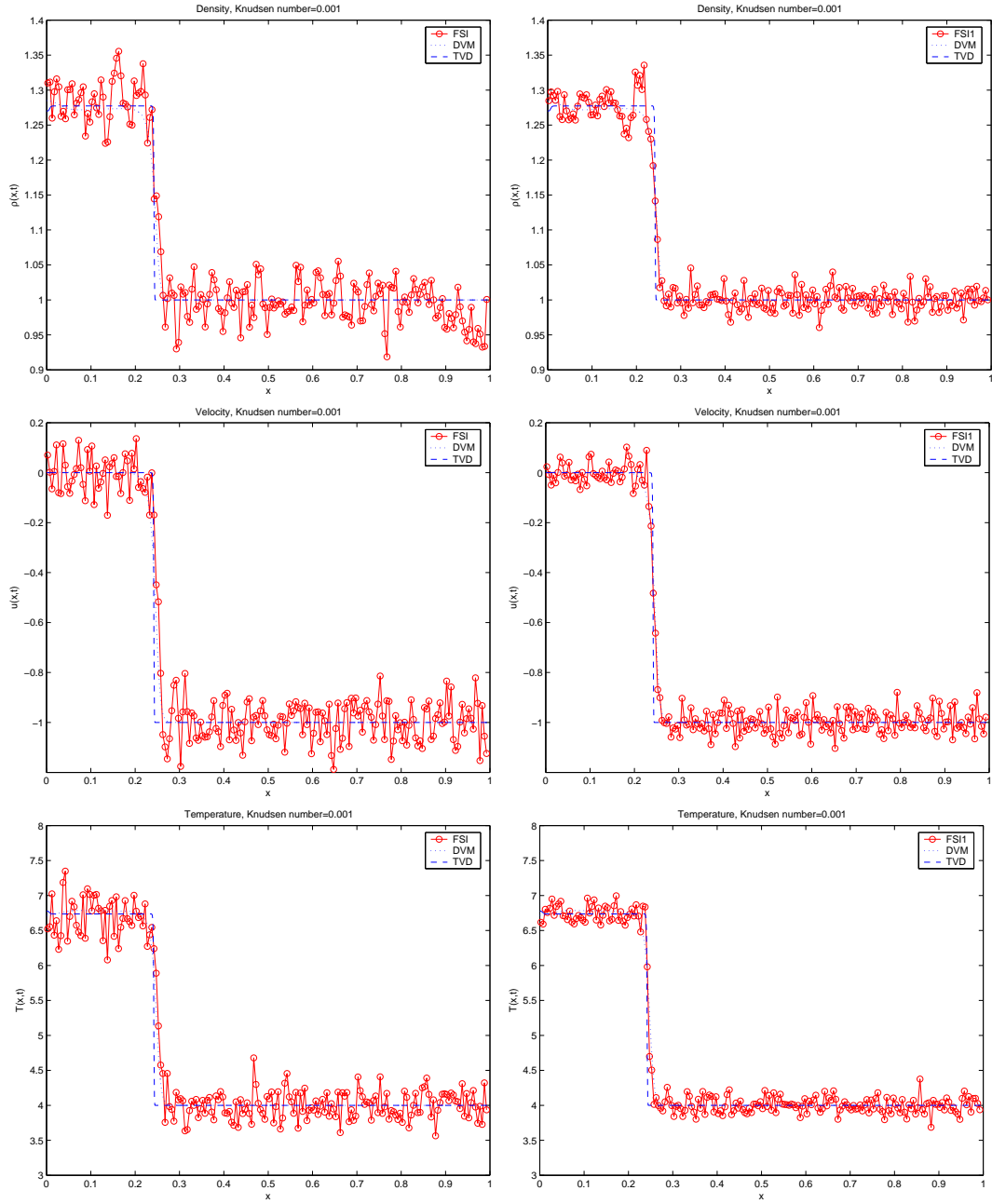


FIG. 5.3. *Unsteady Shock: $\varepsilon = 10^{-3}$. Solution at $t = 0.065$ for FSI (left) FSI1 (right). From top to bottom density, mean velocity and temperature.*

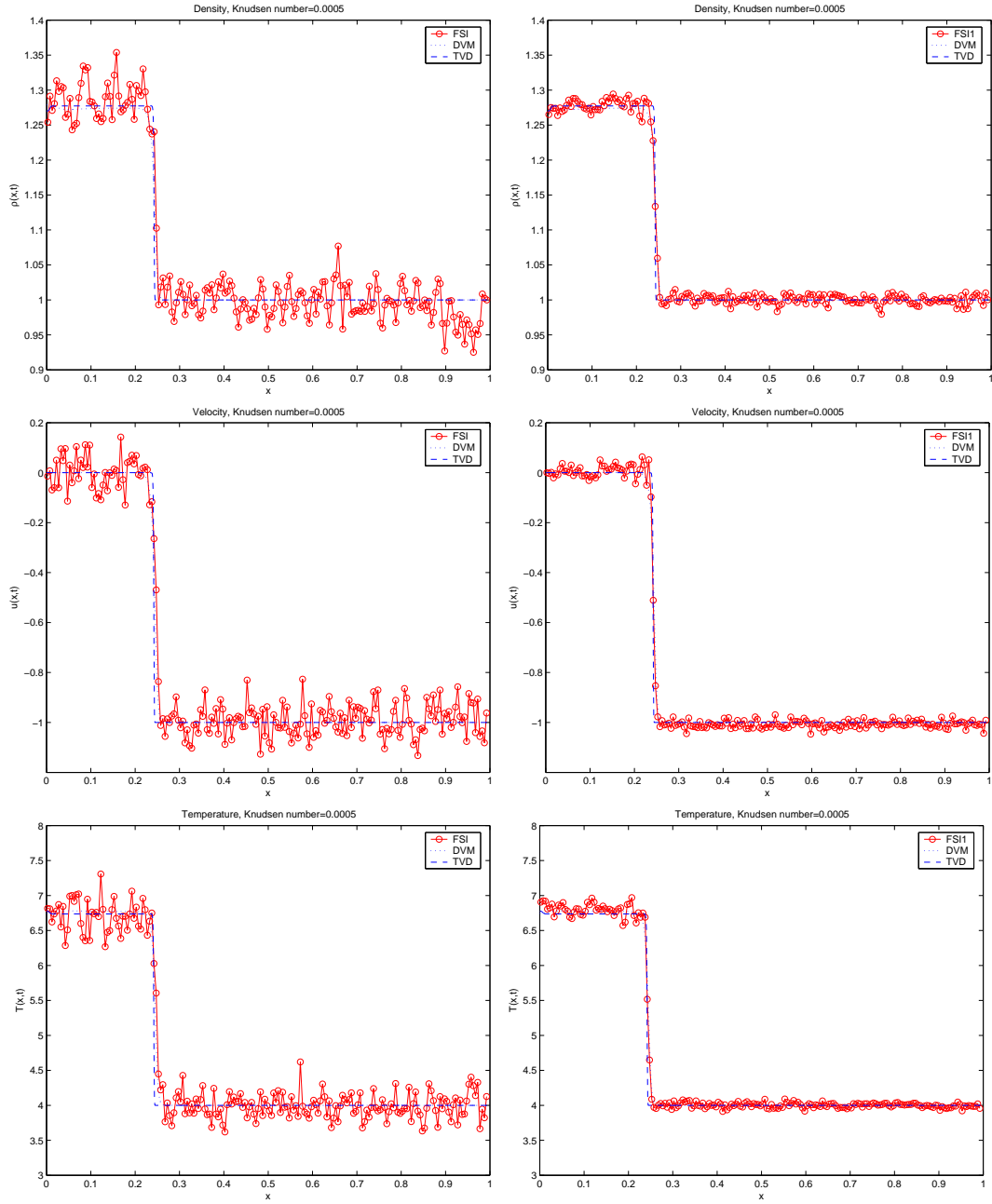


FIG. 5.4. Unsteady Shock: $\varepsilon = 5 \times 10^{-4}$. Solution at $t = 0.065$ for FSI (left) FSI1 (right). From top to bottom density, mean velocity and temperature.

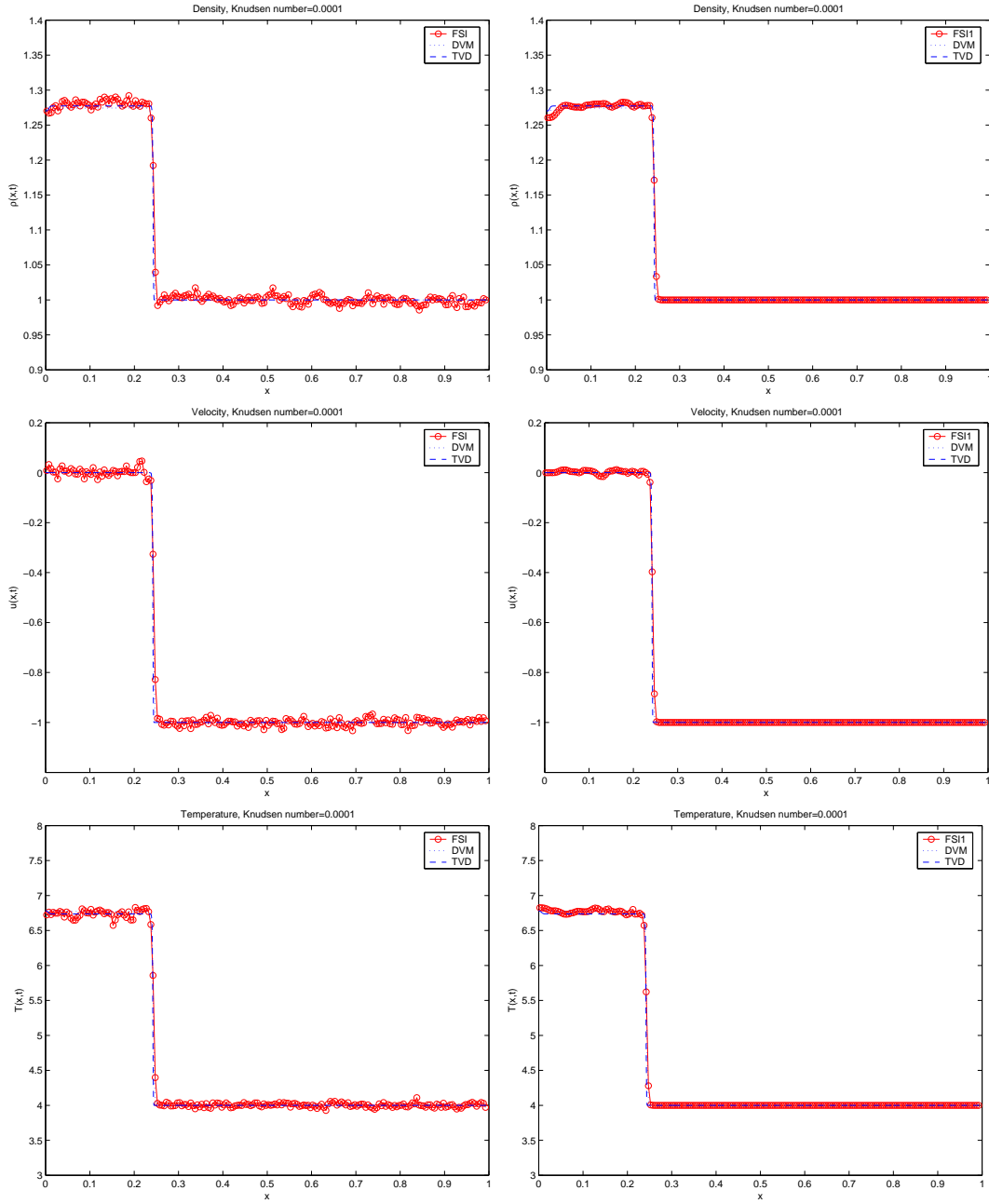


FIG. 5.5. Unsteady Shock: $\varepsilon = 10^{-4}$. Solution at $t = 0.065$ for FSI (left) FSI1 (right). From top to bottom density, mean velocity and temperature.

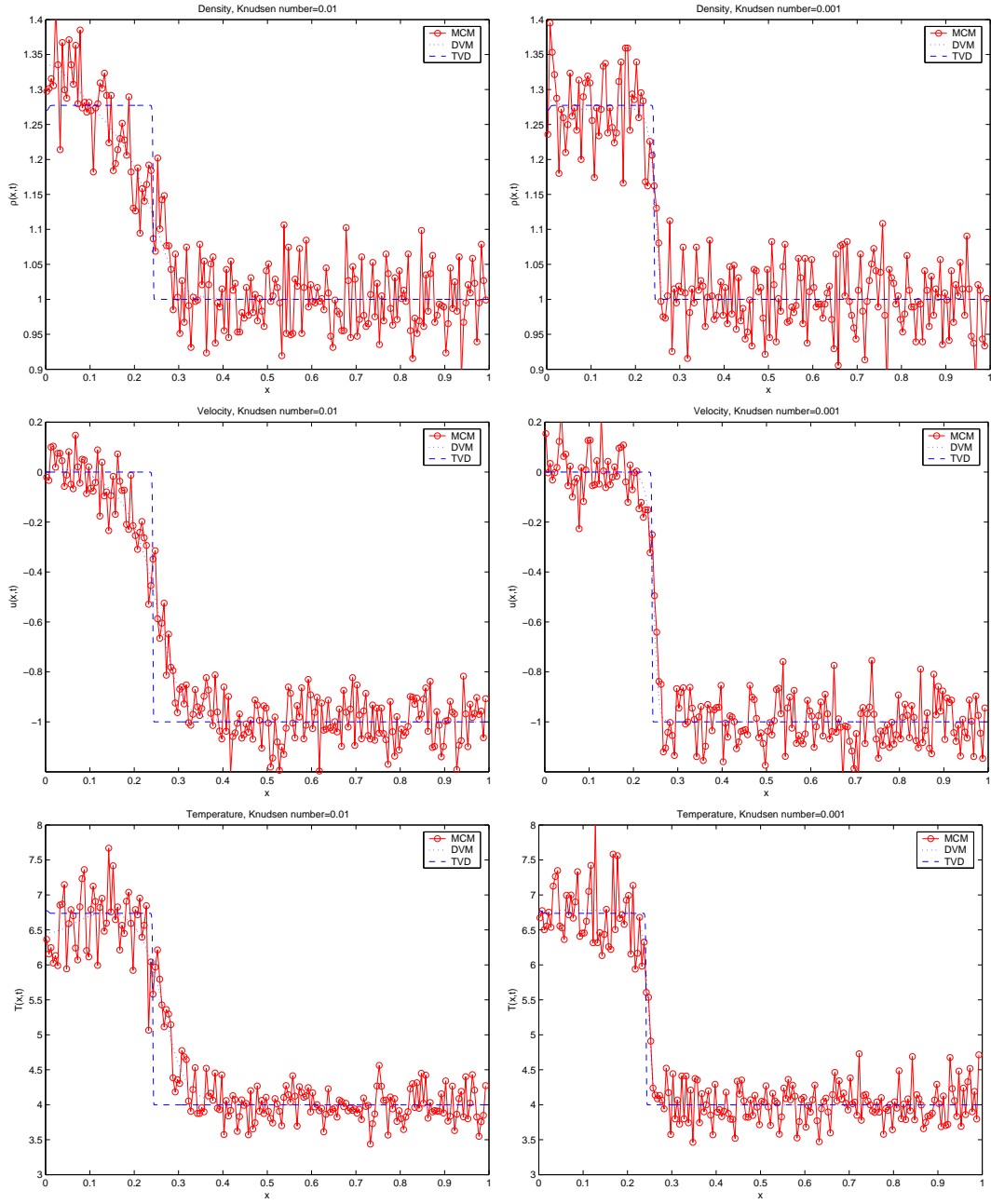


FIG. 5.6. *Unsteady Shock. Solution at $t = 0.065$ for MCM with Knudsen numbers $\varepsilon = 10^{-2}$ (left) and $\varepsilon = 10^{-3}$ (right). From top to bottom density, mean velocity and temperature.*

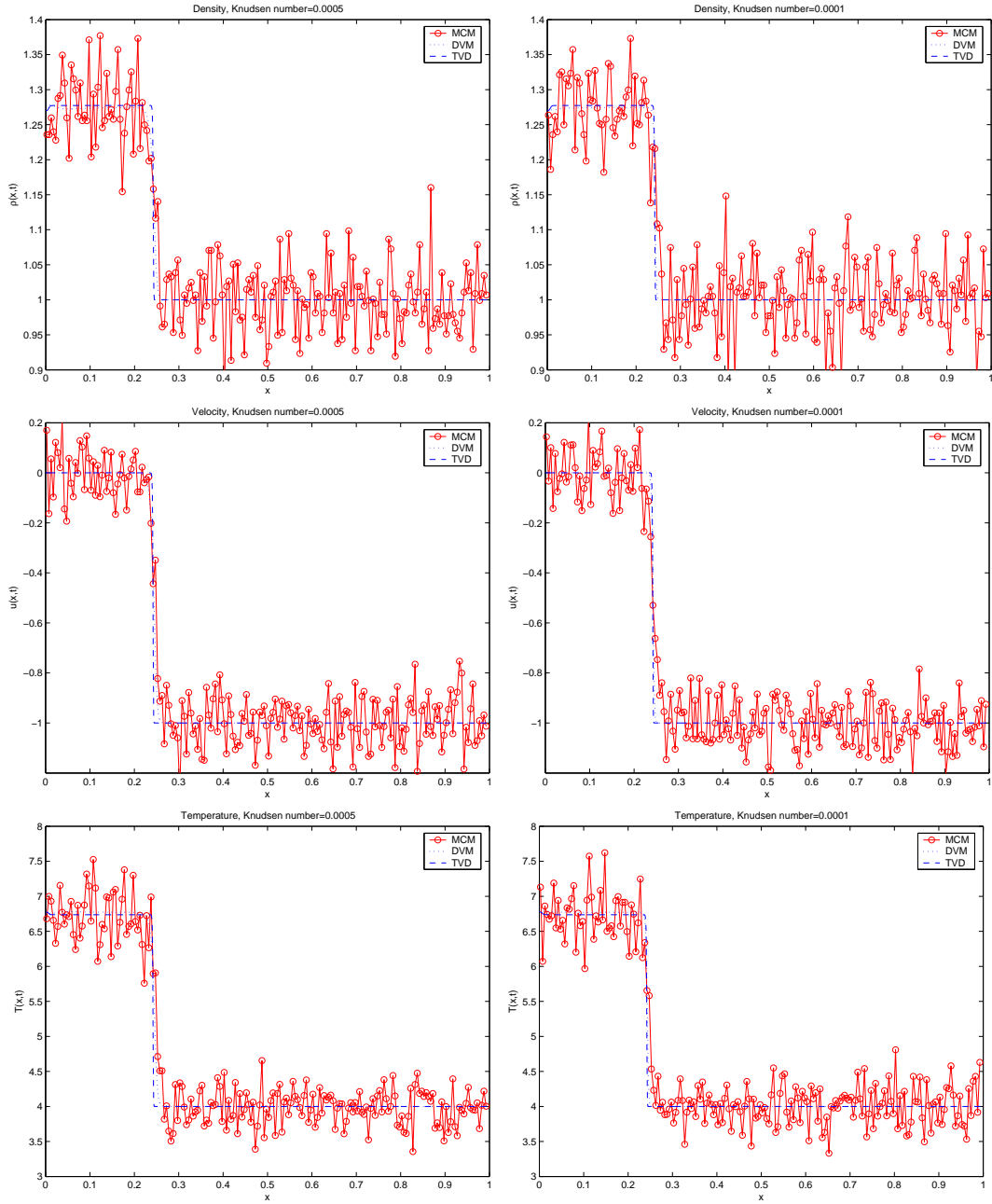


FIG. 5.7. *Unsteady Shock. Solution at $t = 0.065$ for MCM with Knudsen numbers $\epsilon = 5 \times 10^{-4}$ (left) and $\epsilon = 10^{-4}$ (right). From top to bottom density, mean velocity and temperature.*

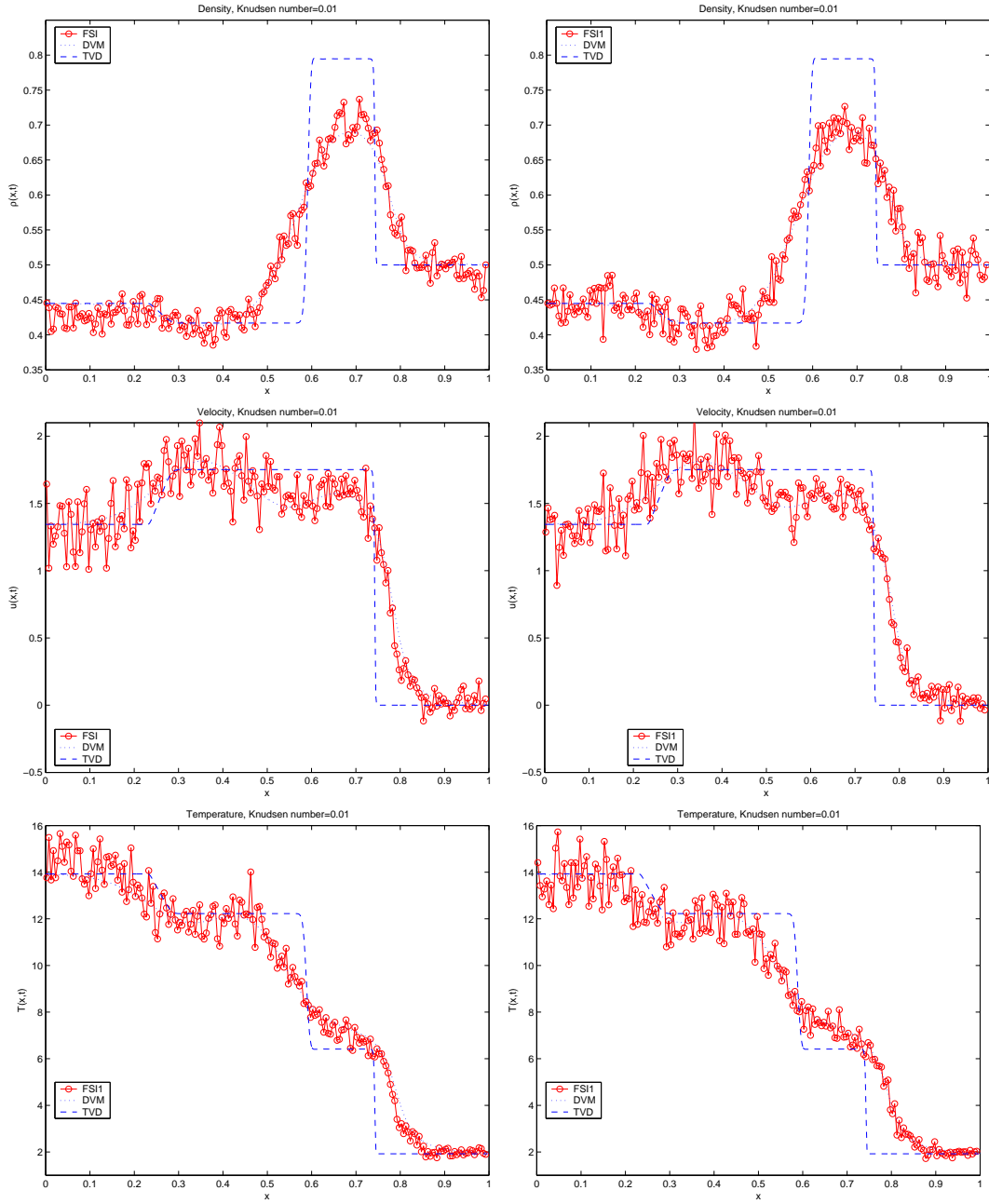


FIG. 5.8. Lax test: $\varepsilon = 10^{-2}$. Solution at $t = 0.05$ for FSI (left) FSI1 (right). From top to bottom density, mean velocity and temperature.

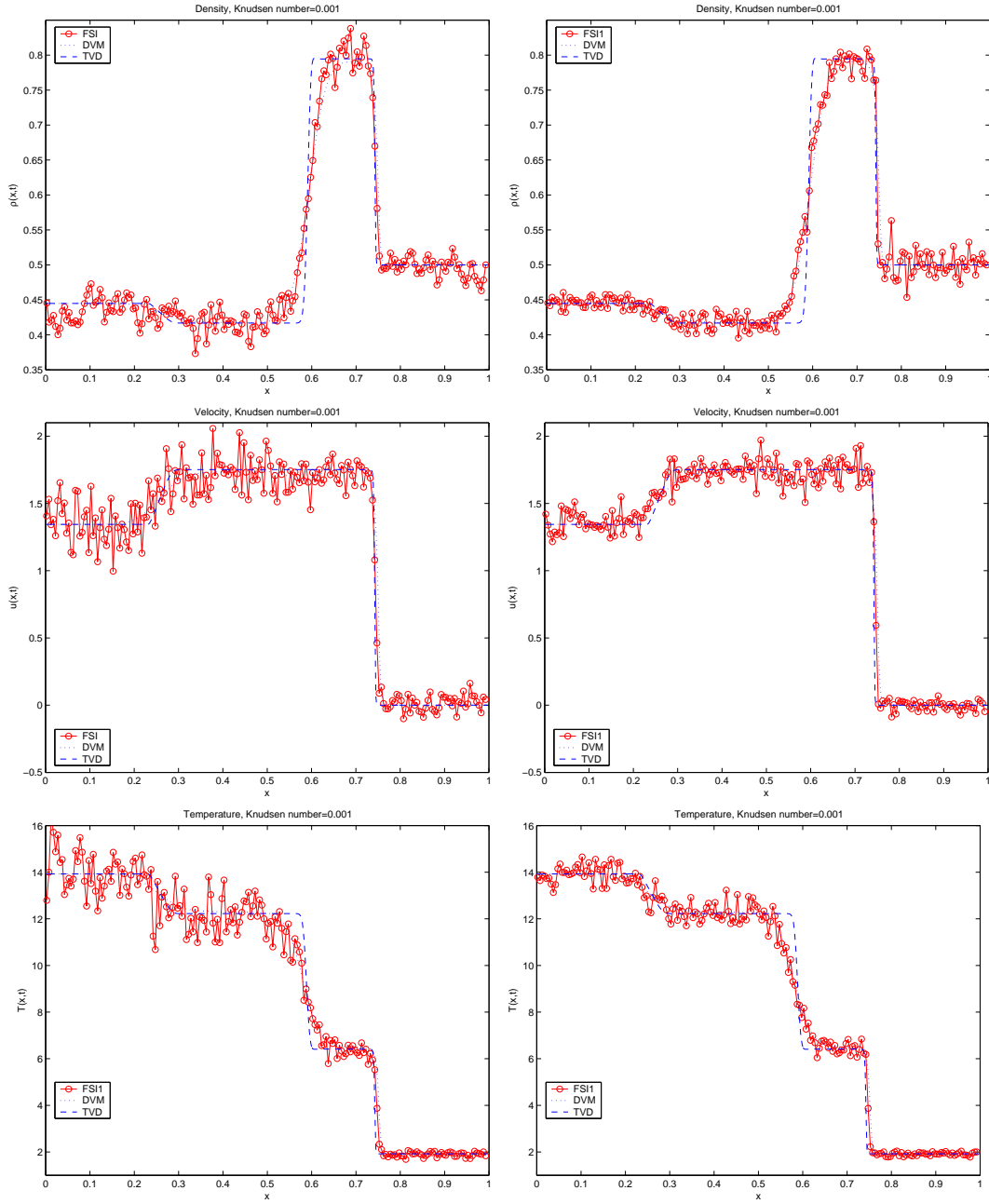


FIG. 5.9. Lax test: $\varepsilon = 10^{-3}$. Solution at $t = 0.05$ for FSI (left) FSI1 (right). From top to bottom density, mean velocity and temperature.

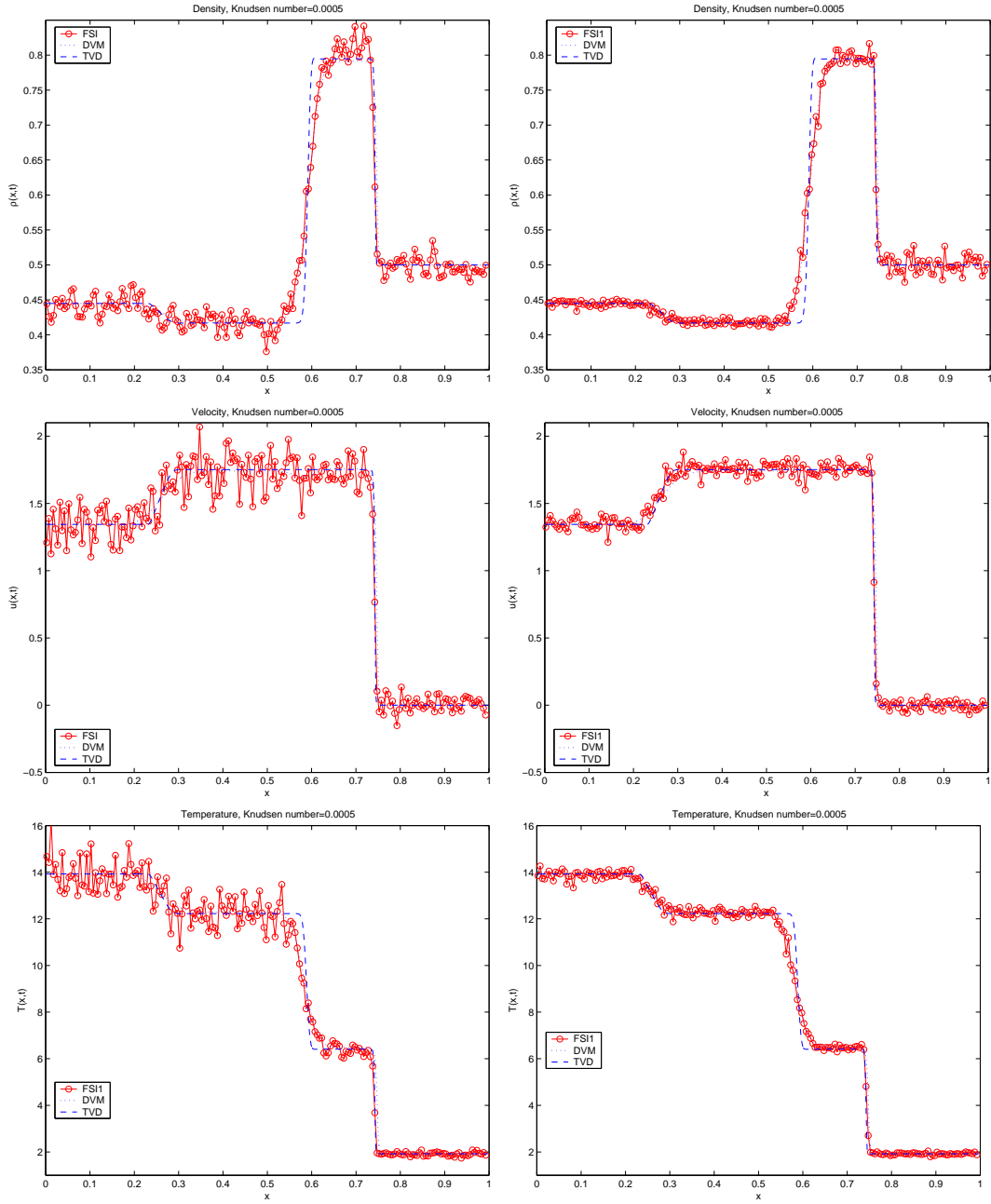


FIG. 5.10. Lax test: $\varepsilon = 5 \times 10^{-4}$. Solution at $t = 0.05$ for FSI (left) FSI1 (right). From top to bottom density, mean velocity and temperature.

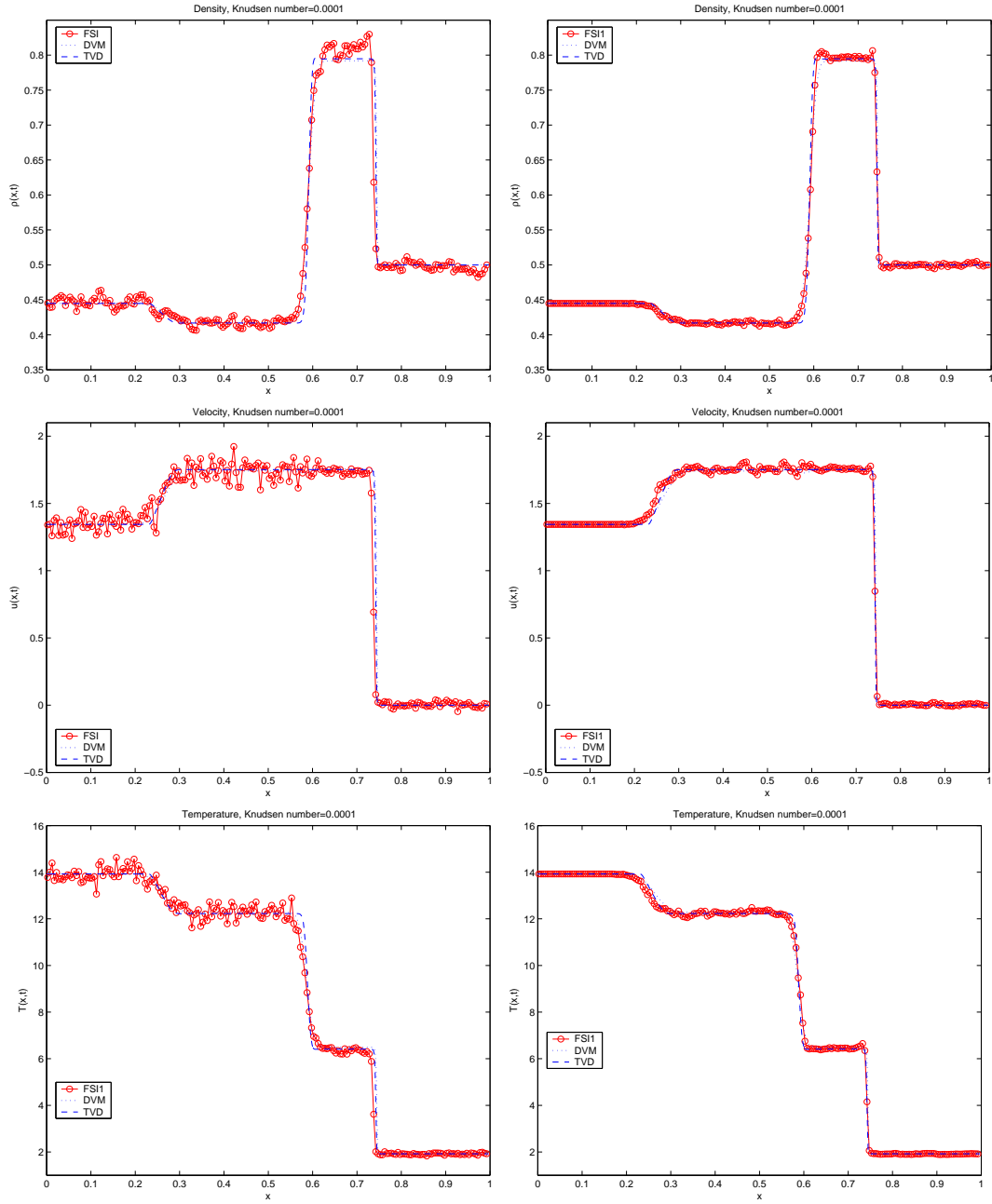


FIG. 5.11. Lax test: $\varepsilon = 10^{-4}$. Solution at $t = 0.05$ for FSI (left) FS11 (right). From top to bottom density, mean velocity and temperature.

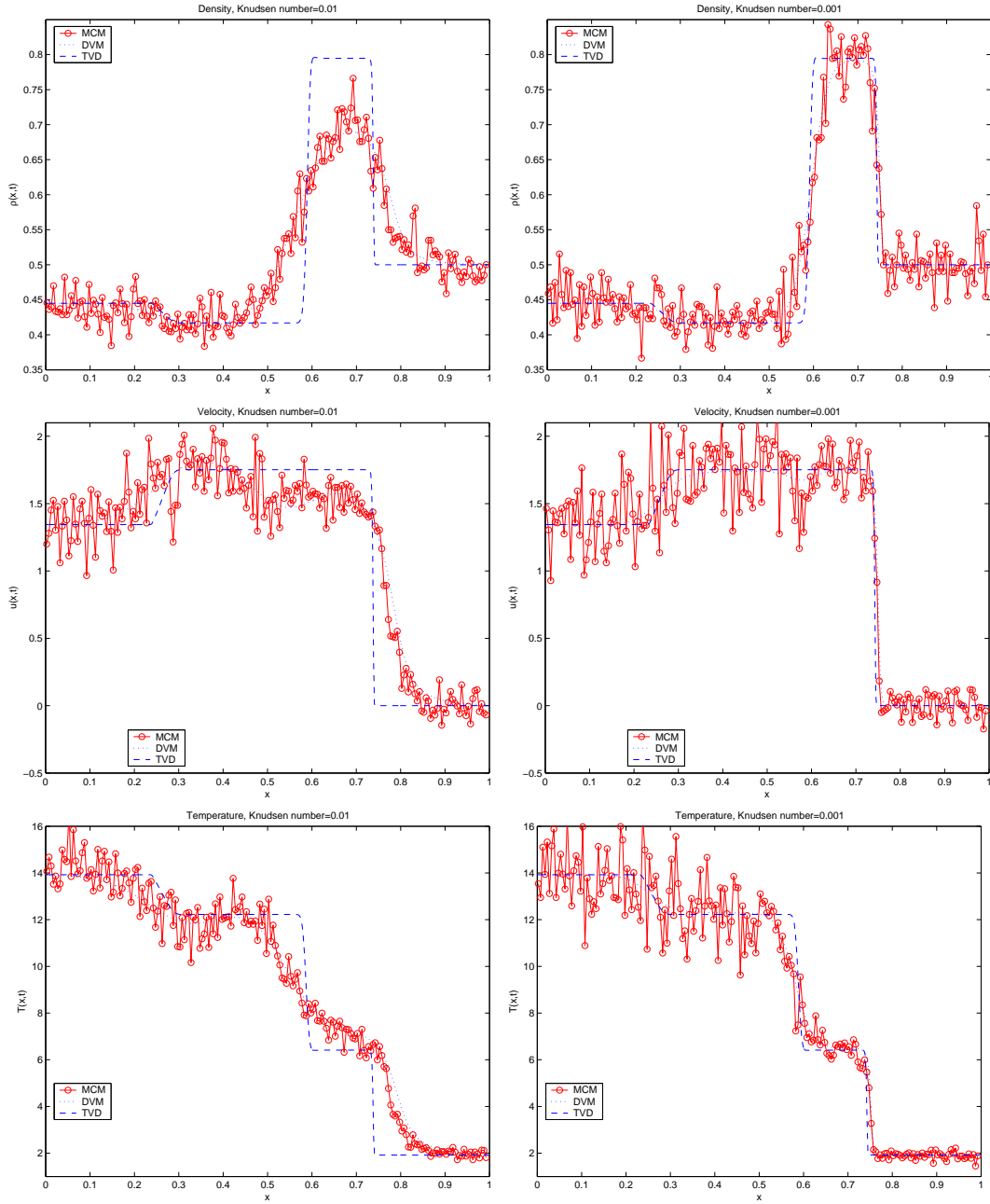


FIG. 5.12. Lax Test. Solution at $t = 0.05$ for MCM with Knudsen numbers $\varepsilon = 5 \times 10^{-2}$ (left) and $\varepsilon = 10^{-3}$ (right). From top to bottom density, mean velocity and temperature.

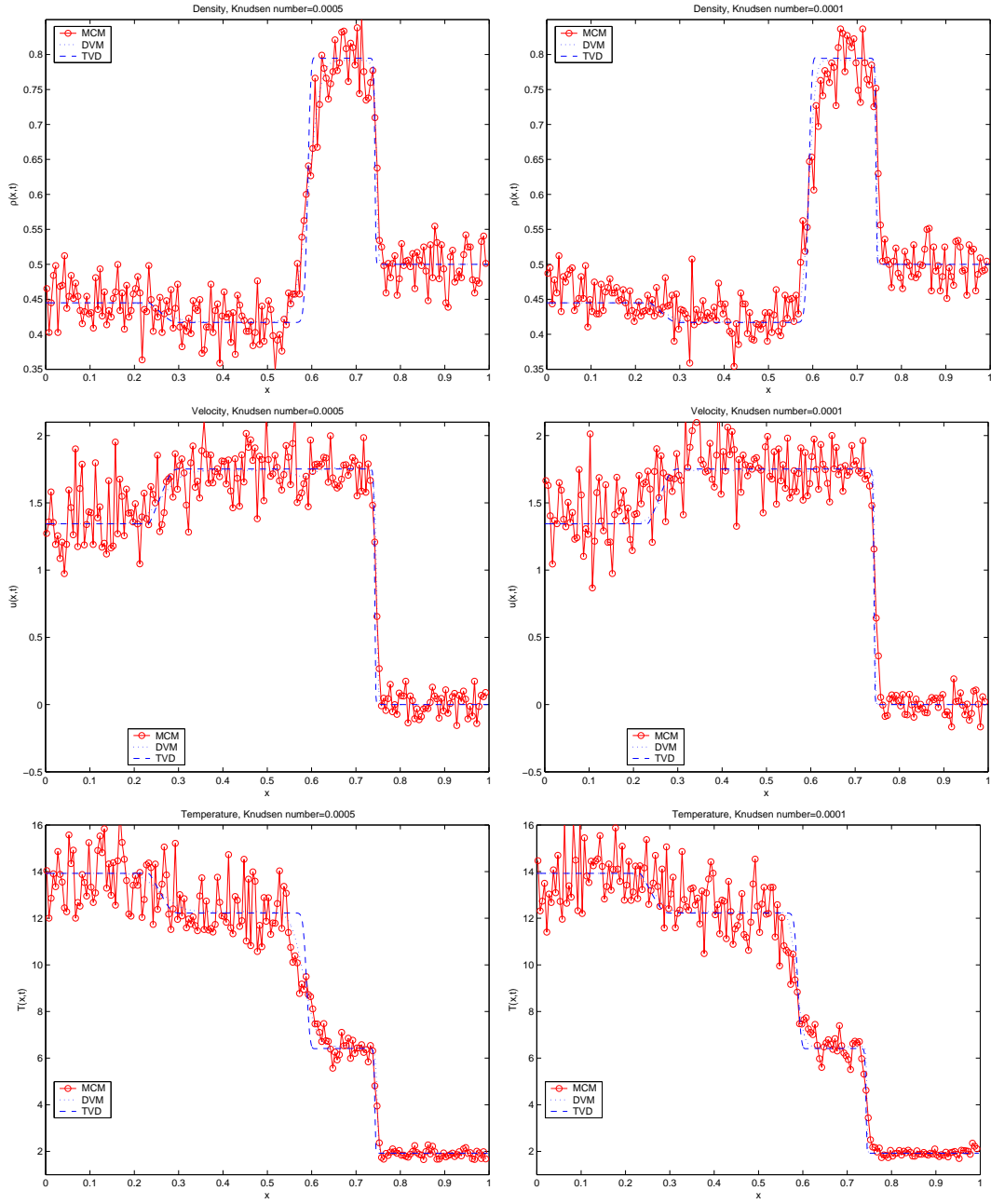


FIG. 5.13. Lax Test. Solution at $t = 0.05$ for MCM with Knudsen numbers $\epsilon = 5 \times 10^{-4}$ (left) and $\epsilon = 10^{-4}$ (right). From top to bottom density, mean velocity and temperature.